Kent Academic Repository

Sun, Jingyuan and Yan, Yong (2016) *Non-intrusive measurement and hydrodynamic characterization of gas–solid fluidized beds: a review.* **Measurement Science and Technology, 27 (11). ISSN 0957-0233.**

Non-intrusive measurement and hydrodynamics characterization of gas-solid fluidized beds – A review

Jingyuan Sun, Yong Yan

School of Engineering and Digital Arts, University of Kent, Canterbury CT2 7NT, U.K.

Email: y.yan@kent.ac.uk

Abstract

Gas-solid fluidization is a well-established technique to suspend or transport particles and has been applied in a variety of industrial processes. Nevertheless, our knowledge of fluidization hydrodynamics is still limited for the design, scale-up and operation optimization of fluidized bed reactors. It is therefore essential to characterize the two-phase flow behaviours in gas-solid fluidized beds and monitor the fluidization processes for control and optimization. A range of non-intrusive techniques have been developed or proposed for measuring the fluidization dynamic parameters and monitoring the flow status without disturbing or distorting the flow fields. This paper presents a comprehensive review of the non-intrusive measurement techniques and the current state of knowledge and experience in the characterization and monitoring of gas-solid fluidized beds. These techniques are classified into six main categories as per sensing principles, electrostatic, acoustic emission and vibration, visualization, particle tracking, laser Doppler anemometry and phase Doppler anemometry as well as pressure fluctuation methods. Trend and future developments in this field are also discussed.

1. Introduction

1.1. Background

Gas-solid fluidized beds are widely employed in industrial processes, ranging from catalytic cracking of petroleum, polymerization, combustion and biomass gasification, to pharmaceutical and food industries. The success of fluidized beds in industry is owing to their excellent heat and mass transfer capabilities [1]. However, the methodology adopted for the design, scale-up, operation and control of fluidized beds still largely relies on experience rather than theory to date. The main reason for this underdevelopment is that the flow structures, phase interactions and multiscale flow mechanisms in fluidized beds are extremely complex and still far from well understanding. Therefore, how to acquire reliable data representing the fluidization properties is an important issue. Meanwhile, the flow field should not be disturbed or distorted during the measurement of the fluidization parameters. Non-intrusive measurement techniques are thus widely required for hydrodynamics characterization. Until now, significant progress has been made in the non-intrusive measurement techniques attributed to the advances in instrumentation, signal processing and computer technologies. However, the accurate measurement and comprehensive description of a fluidization process remain challenging in both technical and scientific fields.

1.2. Nature of gas-solid fluidization

When applying a measuring instrument to a laboratory or industrial gas-solid fluidized bed, the validity and accuracy of the measurement strongly depend on the intrinsic complexity of the flow system, such as the heterogeneous phase distribution, flow regime variation, velocity and acceleration of gas and solid phase, flow disturbance as well as opacity of particles [2]. In essence, such complexity and its effects on the process measurement are dominated by the nature of gas-solid fluidization, which is necessary to be considered before we discuss any specific technique. Moreover, the diversity of fluidized beds gives rise to further complexity and challenges. For instance, with the increase of operating gas velocity, a fluidized bed can perform as the particulate, bubbling, slugging, turbulent and fast (circulating) fluidized beds, which also rely on the particle type (Geldart A, B or D) and bed geometry. In terms of shape, a cylindrical fluidized bed can be referred to as a three-dimensional (3D) fluidized bed, while a rectangular one with the depth much smaller than the height and width is also named a quasi-two-dimensional (quasi-2D) fluidized bed.

1.2.1. Nonlinear and chaotic dynamics

Gas-solid fluidized beds are commonly regarded as nonlinear and chaotic dynamic systems [3], which show both irregular and non-random characteristics and are extremely sensitive to small changes in initial conditions. Two initial states of a system that are almost identical will develop in completely different ways after some

time [4]. That's why a fluidized bed can exhibit different flow behaviours even if it is operated in the same flow regime or under the same condition. In addition, non-linear systems do not follow a single general criterion but tend to converge to certain steady states, many of which are metastable and can transit to new steady states rapidly [5]. Such hydrodynamic characteristics are governed by complicated nonlinear dynamic relationships, which are mainly controlled by different dynamic phenomena occurring inside the bed, including but not limited to bubble formation, bubble coalescence and splitting, bubble passage, particle movement as well as cluster motion [6]. Fluctuating signals of pressure, voidage, electrostatic intensity, temperature and so on are therefore generated and often utilized for flow field analysis. However, due to the complexity, uncertainty and limited predictability of fluidization systems, it is difficult to establish explicit relationships between the measured signals and the hydrodynamic parameters straightforwardly.

1.2.2. Multiscale characteristics and signal hybrid

In view of the fact that a gas-solid fluidized bed is a typical complex system composed of multiscale flow structures, it is often characterized by emergent properties, multiscale interactions, unexpected behaviours and self-organization [5]. The characteristic scales of flow structures range from the individual-particle level to cluster/bubble level and further to bed level. The generation of such diverse flow structures is governed by the compromise between the dominant mechanisms at different scales [5]. Each kind of flow structure evokes certain characteristic signals

during its motion and evolution. Signals produced by different flow structures then hybridize with each other, making the integrated signals even more inexplicable. Moreover, some signals are intrinsically non-local. For example, disturbances in the pressure field of gas phase can be propagated through the bed as a pressure wave. The vibration signals collected by an accelerometer may originate from the vibration sources with different distances from the sensor.

Each measurement technique has its specific temporal and spatial resolutions, while none is capable of providing equally valid information covering the whole spectrum of scales and describing complete features of a multiscale flow system [7]. Owing to the hybrid and multiscale characteristics of the flow signals, it is logical to combine different techniques together to obtain the hydrodynamic information at different scales simultaneously. Furthermore, decoupling the raw signals is another important step for information extraction.

1.2.3. Particle backmixing

Different from the unidirectional solids flow in pneumatic transportation pipelines, strong backmixing of particles often occurs in gas-solid fluidized beds, especially under the dense-phase flow conditions. Particle backmixing can be caused by different flow behaviours. Firstly, the rising bubbles carrying particles in their wakes erupt above the bed surface, leading to particle falling along the wall. Secondly, the shear of gas jet and bubbles may enhance the particle backmixing in emulsion phase. Thirdly, the formation and breaking of particle clusters also strengthens particle

backmixing. Under the influence of particle backmixing, it is difficult to measure the solids velocity accurately (The term *solids velocity* here stands for the average of all instantaneous particle velocities within the sensing area, while the term *particle velocity* represents the instantaneous velocity of an individual particle). For example, electrostatic induction sensors are commonly used to measure the bulk solids velocity in unidirectional flow. Yet in a dense-phase fluidized bed, they are only sensitive to the movement of backmixing particles near the wall, without any information provided about the solids flow in the central region. Particle image velocimetry (PIV) technique is rarely applied on a 3D dense-phase bed with strong particle backmixing, since the image quality of solids flow field in the central region is significantly influenced by the particle curtains near the wall.

1.2.4. Particle size distribution and particle shape

According to the Geldart particle classification criterion [8], particles in gas-solid flow systems are categorized into A, B, C and D groups based on their diameters and densities. Particles belonging to different groups exhibit significantly different fluidization properties. Apart from the mean diameter, particle size distribution also affects the flow hydrodynamics. A wider size distribution gives rise to increased bed expansion, decreased incipient fluidization velocity, higher minimum bubble velocity and smaller bubbles with more gas passing through the emulsion phase [9]. Different distributions result in distinct solids mixing patterns such as complete mixing, partial mixing, particle segregation and defluidization [10]. Although the particle size

distribution can be easily obtained through an off-line sieving method or a laser particle analyzer, few techniques are available for the on-line measurement and monitoring of it. In addition, particles in many industrial fluidization processes are non-spherical, such as the highly-elongated biomass particles for the thermochemical conversion to syngas [11]. Particle shape and orientation affect the voidage and solids velocity distribution. However, little attention has been paid in considering such influences. It is even more difficult to measure the particle shapes on-line continuously in a flow process using specific instruments.

1.2.5. Hot and dusty conditions

Attributed to the excellent capability of heat transfer, gas-solid fluidized beds serve as ideal reactors for exothermic reactions [12]. As a consequence, the sensors and devices installed on industrial fluidized beds are required to withstand harsh conditions. For example, the temperature inside an industrial fluidized bed boiler can reach as high as 950℃ [13], which makes some conventional sensors ineffective. In such a boiler, the flame produced by coal combustion may also distort the flow field, giving rise to low signal-to-noise ratios. In addition, the suspended dust may affect the operation of optical sensors as the dust can contaminate the optical access windows, obstruct the illumination light and even block the sensing paths.

1.3. Scope and structure of this review

Measurement techniques applied in gas-solid fluidized beds can be characterized as either intrusive or non-intrusive. The intrusive ones based on optical fiber probes,

hot film anemometry, conductivity probes and thermocouples all suffer from a disadvantage of disturbing the flow field and hence the accuracy of measurement results. This review presents only the non-intrusive techniques, including their sensing principles, characteristics and current developments. Signal processing strategies are also introduced where appropriate. There have already been some reviews concerning the relevant topics in this field. For example, Yan [14] presented a comprehensive review of non-restrictive techniques for the mass flow measurement of pneumatically conveyed solids. Werther [15] introduced measurement techniques applicable to fluidized beds with a focus on intrusive probes, although non-intrusive techniques, such as Laser Doppler anemometry, gamma-ray tomography, and positron emission particle tracking, were also briefly reviewed. Tayebi et al. [16] reviewed the measurement techniques for multiphase flow systems, yet aiming at the flow diagnosis and averaging procedures for simulation validation rather than the measurement and monitoring of fluidization processes. Moreover, significant developments of the non-intrusive techniques have emerged in recent years. This review, covering both the current and recent work over a wide range of topics, is presented in a systematic way under six main categories, electrostatic, acoustic emission and vibration, visualization, particle tracking, laser Doppler anemometry and phase Doppler anemometry as well as pressure fluctuation methods.

2. Electrostatic methods

Electrostatic phenomena exist widely in gas-solid fluidization processes. They are

originated from frictional charging, tribo-electrification and contact charging, which are induced by the particle-particle, fluid-particle and particle-wall contacts and frictions [17]. The measurement of electrostatic charges allows the characterization of different flow properties in a fluidized bed. Firstly, since the charge accumulation significantly affects the fluidization operation and can cause particle agglomeration, electrostatic discharge and even reactor shutdown [18, 19], it is essential to quantify the electrostatic charges for the purpose of monitoring and control. Until now, extensive work has been undertaken to measure particle electrostatic levels in gas-solid fluidized beds [20-26]. Secondly, based on the relationship between electrification and solids motion, the electrostatic techniques have been commonly applied in pneumatic transport pipelines to measure the velocity, concentration and mass flow rate of solids phase [14, 27-33]. However, developments of these techniques for the characterization of flow parameters in gas-solid fluidized beds are limited [34, 35].

The instruments employed to measure the electrostatic charges in fluidized beds are classified as electrostatic sensors and Faraday cups. The electrostatic sensors include both contacting (or collision) probes and induction sensors [36]. A contacting probe in the form of a ball, hemisphere or rod is inserted into the bed and allows direct charge transfer and measurement between the particles and the probe. It is thus intrinsically intrusive and suitable for the electrostatic signal collection from the bed center to the wall. However, the limitations of a contacting probe are the extra charge generation due to the particle collision and adhesion, as well as the disturbances to the

flow field [17]. Therefore, the signals from a contacting probe should be used for qualitative analysis rather than quantitative measurement of flow parameters. Nevertheless, owing to the capability of offering information about charge distribution, particle charge-to-mass ratio and even bubble rising velocity, contacting probes have been applied more commonly than induction sensors on gas-solid fluidized beds [19, 22, 37-39]. In this review, we will focus on the non-intrusive induction sensors.

2.1. Electrostatic induction sensors

Electrostatic induction sensors, based on the electrostatic induction principle, perform as a simplest type of field meter. They are immune to extra charge transfer and are independent of net charge accumulation such as with contacting probes. The output of an electrostatic induction sensor is in the form of an induced charge signal [40, 41], current signal [26], or voltage signal [35, 42], based on which the charge distribution and charge level in a gas-solid fluidized bed are obtained. In addition, the solids velocity and relative concentration can be characterized through electrostatic signal processing. Fig. 1 shows the installation diagram of an induction sensor used to measure the charge distribution around a rising bubble [40]. The sensor is made of an insulated and circular copper disc (10 mm diameter), connected to the core of a coaxial cable, embedded in a Teflon cylinder and wrapped with a single strip of conducting copper tape. The sensor is mounted flush with the outer wall to avoid direct contact with particles. It is known that the movement of particles surrounding a rising bubble is fiercer than that in the emulsion phase, resulting in stronger

10

interaction among the particles and more charge generated around the bubble. When a bubble passes the sensor, the variation in the induced charges is measured, with an opposite sign to the variation of particle charges in front of the sensor. The charge distribution around a bubble was then reconstructed from the signals collected by four sensors radially placed on the rising path of the bubble [40, 41]. However, such induction sensor is only applicable to quasi-2D fluidized beds, since in a 3D bed, the charges on particles away from the wall cannot be measured accurately due to the limited spatial sensing range of the sensor. In addition, it is unlikely to determine the absolute charges on particles directly from the induced electrostatic signals, which are dependent on solids velocity and concentration.

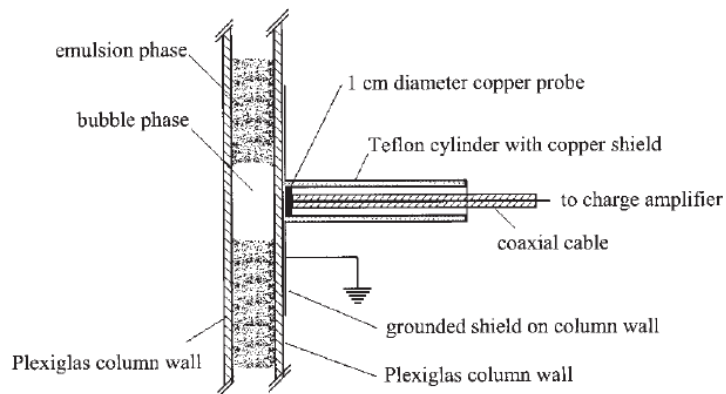**Fig. 1. Installation of an electrostatic induction sensor [40]**

Apart from the induction sensor with a disc shape, the arc-shape ones have also been applied to gas-solid fluidized beds recently. Zhang et al. [35] measured the solids velocity at different positions in a bubbling bed by utilizing induction sensor arrays. Each sensor array has three layers, each consisting of four identical arc-shape

electrodes with an equal spacing. Signals from the sensor array were processed through cross correlation to obtain the solids velocity. However, due to the chaotic motion of particles in a dense-phase bed, the measurement accuracy is significantly influenced by the strong backmixing of particles, and the correlation velocity only reflects the activity of particle motion close to the wall. Dong et al. [26] further adopted a similar sensor array to measure the relative charge level in a bubbling bed based on the recorded induced current. Nevertheless, since the current amplitude depends not only on the charges on particles but also on the solids velocity and concentration, the measured 'charge level' only qualitatively represents the particle charges without taking the influences of solids velocity and concentration into account.

Induction sensors used in pneumatic transport systems are made of ring-shape, arc-shape and stud-shape electrodes [27]. Although they are usually exposed to the gas-solid flow during the measurement, the triboelectric charging and charge transfer between the particles and the sensors can be significantly reduced by mounting the sensors flush to the inner walls. In addition, compared to a contacting probe, it is easier to reconstruct the charge distribution from the signals, since the influences of contact charging can be reasonably ignored in this situation. However, as mentioned above, induction sensors are suitable for indicating the variation of particle charges rather than measuring their absolute value, and the spatial sensing ranges are confined near the wall. The measurement accuracy is thus affected by the particle backmixing near the wall. Besides, induction sensors are susceptible to drift and distortion. Special

designs are therefore needed to overcome these problems [40]. Moreover, it is difficult to embed the ring-shape and arc-shape electrodes in the walls of industrial fluidized beds. Due to these limitations, further modifications and developments of induction sensors are required to improve the measurement reliability for the dense-phase and industrial fluidization systems.

2.2. Faraday cups

Faraday cups have been employed to directly measure the cumulative net charges on fluidized particles, based on which the particle charge-to-mass ratio is obtained [17, 23, 43]. Since the fluidizing gas needs to be cut off to record charges on the dropped particles, most Faraday cups can be considered as intrusive and off-line devices [17, 23, 43]. Until now, the only 'non-intrusive' Faraday cup seems to be the one developed by Mehrani et al. [20, 44], as shown in Fig. 2. The bed itself is employed as the inner Faraday cup and a second column as the outer cup. Three sections made of different materials constitute the inner column with 0.1 m diameter and 2.1 m height. The middle section made of copper is connected to the both ends of the Teflon sections and to an electrometer to measure the charges induced on the column wall. The top expanded section made of Plexiglas is to reduce the entrainment of fine particles. The copper outer column is grounded to eliminate the external electrical interferences. It was shown that the fine particles leaving the bed resulted in the build-up of net charges inside the bed, while the charging effects of the particle-gas contact and gas ionization were negligible. Although the conventional Faraday cups

suffer from strong interferences to the flow field and generation of extra charges when handling particles, this 'non-intrusive' Faraday cup has no such drawbacks. However, the approach only allows the measurement of total net charges in a fluidized bed and is thus unable to provide any information about the charge distribution on particles.
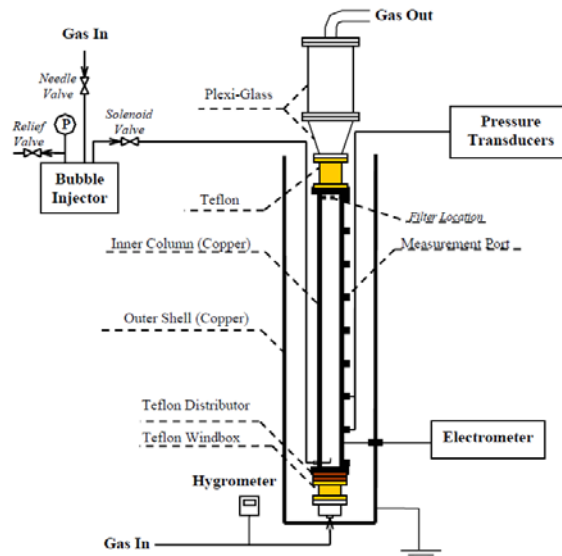
Fig. 2. A 'non-intrusive' Faraday-cup measurement system [44]

It is known that, due to the complex nature of electrostatic phenomena, the electrostatic signals collected from a fluidized bed are dependent on many factors, such as solids velocity, solids concentration, particle properties (e.g. size, shape, hardness), humidity and temperature. Therefore, it is important to decouple and extract different hydrodynamic information from the electrostatic signals. For instance, the solids velocity is measured through a pair of axially spaced electrostatic induction sensors in combination with cross-correlation processing. Such measurement is principally independent of the signal amplitude, free from variations in particle

properties and humidity, and suitable for a wide range of flow conditions. Signal processing electronics with an automatic gain control mechanism can also be used to maintain an optimum signal range [27]. In addition, the relative solids concentration is indicated by the root mean square of electrostatic signals [42]. The particle size can be determined through the combination of electrostatic sensors and piezoelectric sensors [45]. Normally, particles are fluidized for 20~30 min prior to electrostatic measurement to achieve a saturated charged state, and the particle species, humidity and temperature are kept unchanged during the measurement. By this means, the influence of other parameters on the electrostatic measurement is eliminated or reduced.

3. Acoustic emission and vibration methods

Acoustic emission (AE) and mechanical vibration measurement techniques are both useful tools for monitoring process status and characterizing dynamic parameters. Although the setup of AE and vibration measurement is quite different for various processes, their basic equipment is similar [46]. A sensor or a sensor array is used to collect the acoustic pressure fluctuation/vibration signals, which are then amplified with the undesired frequency components filtered out. The amplified signals are finally converted into a digital form for display on an oscilloscope or analysis on a spectrum analyzer or a computer. In the following sections we will review and discuss the AE and vibration techniques applied to gas-solid fluidized beds.

3.1. Acoustic emission sensors

Acoustic emission (AE) caused by the physical and chemical events occurring in a process can provide valuable information about what is happening in the process [46]. AE measurement hence allows the real-time, on-line and non-intrusive monitoring of a process without direct contact to the vessels or pipelines. Two methods are commonly utilized for the implementation of AE measurement. The first is the active AE technique, in which a high-frequency acoustic wave is transmitted through the material under test and the changes in the attenuation and speed of sound are measured, in order to monitor the process status. This method has been widely applied in the food processing industry, as reviewed by McClements [47]. The second method is the passive AE technique, in which the acoustic signals produced by the process itself are acquired and analyzed to characterize the flow behaviours. There have been attempts to apply this technique to the on-line monitoring of gas-solid fluidized beds. However, many challenges remain to be resolved, particularly in the interpretation of and the hydrodynamic information extraction from AE signals. This review will focus on the applications of the passive AE technique to gas-solid fluidized beds.

3.1.1. Microphones

Audio in the air (frequencies in 20 Hz~20 kHz) can be sensed by a microphone, which converts the acoustic signals into electrical ones. Some microphones employ piezoelectric crystals for the signal conversion, while others (e.g. condenser

microphones) are based on the principle of capacitance sensing. In a condenser microphone, a thin membrane is exposed to the sound field and the movement of the membrane alters the spacing of a parallel plate capacitor. The changes in capacitance then result in the changes in the voltage across the capacitor [46]. A typical setup of the microphone measurement applied on a gas-solid fluidized bed is shown in Fig. 3. In this case two microphones are fitted to two circular mounted surfaces that are inclined 60° above the horizontal plane to improve the recording quality. Signals from the microphones are amplified through a mixing console and sent to a data logger where the signals are digitized [48]. Zukowski [49, 50] used a single microphone on a bubbling fluidized bed to collect the AE signals generated by the combustion of premixed natural gas and air. The combustion occurring position and the bubble explosion pattern were analyzed directly from the signal shape, while the frequency of bubble explosion was determined through a special algorithm. Although this work sheds some light on the on-line measurement of bubble behaviours, the information obtained is still insufficient to characterize the complex flow dynamics inside the fluidized bed. A main factor that affects the reliability and accuracy of the measurement is the strong background noise. Therefore, signal processing methods should be applied to extract valid information from the raw AE signals. For example, time domain analysis, frequency domain analysis and state space analysis methods were employed to characterize the dynamic properties in a slugging fluidized bed [48]. Moreover, microphones have been utilized to identify initial and full minimum fluidization states [51], as well as to determine the fluidization quality during a drying

process [52].
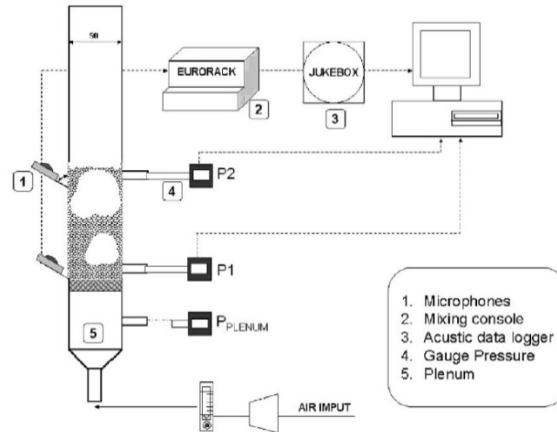
Fig. 3. Microphone measurement system [48]

Microphones are simple, low-cost and non-intrusive measurement devices and are easy to install on fluidized beds. However, they have several significant disadvantages. Firstly, they should be located externally to the fluidized beds, which makes the AE signals easily contaminated by background noise, mechanical vibration and bed response. Secondly, microphones are unsuitable for the measurement of local flow parameters due to their low spatial sensitivity and resolution. Therefore, the differences in the frequency characteristics of the signals at different locations can hardly be identified through a single microphone or a microphone array. Thirdly, the vibration signals generated by particle motion cannot be collected by a microphone, which results in loss of information about the solids flow.

3.1.2. Piezoelectric acoustic sensors

An acoustic sensor is a device that converts the acoustic pressure fluctuation to an

electric current. The most commonly used AE sensors in gas-solid fluidized beds are based on the piezoelectric effect of piezoelectric crystals, which produce small electric charges when acted upon by pressure fluctuation [46]. Compared to accelerometers, AE sensors are more sensitive to the higher-frequency signals generated by particle collision and friction, and hence more suitable for the measurement and monitoring of the particle-related hydrodynamic parameters. A typical AE measurement system applied on a gas-solid fluidized bed is schematically shown in Fig. 4. The sensor is normally mounted on the outer wall of the bed. Jiang et al. [53] proposed a main frequency model to determine the average particle size in a fluidized bed from the power spectrum of the AE signal. The model is expressed as,

$$\bar{f} = \frac{2}{5.7} \left[\frac{(U_s D_0)^{1/5}}{D^{2/5} \overline{d_p}^{6/5} \rho_s^{2/5}} \right] \tag{1}$$

where $\bar{f}$ represents the main frequency of the AE signal, U_s the superficial gas velocity, D_0 an empirical constant, D the elastic modulus constant, $\overline{d_p}$ the average particle diameter, ρ_s the particle density. It was found from a series of experiments on industrial beds that the deviation of particle sizes through the main frequency model and through the conventional sieving method was less than 8.8% [53]. Moreover, the frequency distribution of AE energy was used to predict the agglomeration occurrence in a laboratory bed. When an artificial agglomerate was added, the dominant frequency range of the AE energy moved from microscale (15.63~250 kHz) to mesoscale (3.92~16.53 kHz). Although this work does not provide accurate prediction of the particle size, it has been demonstrated that the AE

sensor is promising for the on-line monitoring of particle size and agglomeration occurrence. Furthermore, the multiscale characteristics of AE signals was interpreted in detail by He et al. [7]. The AE signals were decomposed via wavelet transform into the macroscale, mesoscale and microscale components, based on which a prediction model of particle size distribution was proposed. The average absolute deviation of the particle size distribution obtained through the model from that through the sieving method was no more than 2.14%, while the relative deviation of the average particle size was no more than 4.69%. It was also shown that the AE signals mainly represent the particle motion at microscale as well as the dynamic interactions between the particles and bubbles at mesoscale. This work has proven the advantage of wavelet transform for the prediction of particle size distribution over Fourier transform. Subsequently, Ren et al. [54] applied the same model to an industrial fluidized bed and predicted the onset of particle agglomeration based on the abnormal particle size distribution.
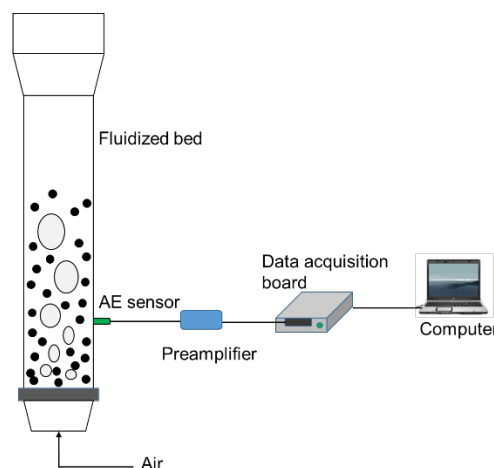

Fig. 4. Acoustic emission measurement system

Apart from the particle size prediction, AE sensors have been utilized to characterize the solids flow pattern and bubble dynamics in gas-solid fluidized beds. Different flow patterns such as the multi-circulation and single circulation were identified based on the axial profiles of the time-averaged AE energy [55]. Similarly, the temporal distribution and derivative of the AE energy were used to determine the flow regime transition, the minimum fluidization velocity as well as the onset of turbulent fluidization [56]. In addition, information about the bubble dynamics was obtained from the envelope of the AE signals, such as the position, velocity and frequency of bubbles [57]. It was found that more reliable estimation of the bubble velocity was achieved by the AE measurement instead of the pressure fluctuation measurement, due to the more complex compositions and less localization of the pressure signals. Besides, at the bed surface, AE signals were still strong and sensitive to the bubble motion, while the pressure signals became quite weak [57].

AE sensors have advantages of versatility, small dimension, wide frequency range, high temporal resolution, low cost and robustness. Since they are sensitive to the microscale and mesoscale flow signals that represent the particle motion and particle-related interactions, it is logical to characterize the particle-level flow hydrodynamics through AE measurement in combination with the multiscale analysis methods (e.g. wavelet transform). However, the widespread application of AE sensors still faces several challenges. Firstly, the sampling rates of AE sensors must be high enough in order to capture the flow signals at high-frequencies, which makes it necessary to use high-performance data acquisition systems for data logging and

processing, especially when an AE sensor array is adopted to collect multiple signals simultaneously. Secondly, AE signals are often hybrid and may originate from different sources, including background noise. It is therefore important to develop the signal processing techniques to accurately extract the characteristic information about various flow behaviours from the raw signals. Thirdly, since assumptions or simplifications are often used when modeling a process based on the AE signals, the reliability of the predicted results is sometimes doubtful.

3.2. Accelerometers

Mechanical vibration can be considered as an oscillatory motion about a reference position, which can further generate waves and *vice versa* [58]. In order to obtain the information about the physical phenomena encoded in the vibration, it is necessary to characterize the oscillatory motion in terms of both amplitude and frequency. An accelerometer is a device to measure the acceleration of the vibration experienced by an object. The particle motion and bulk dynamics in gas-solid fluidized beds can thus be characterized using accelerometers. Since the measurement setup of an accelerometer on a fluidized bed is similar to that of an AE sensor, its schematic diagram is omitted to avoid duplication.

3.2.1. Characterization of particle motion

The particle motion in a gas-solid fluidized bed always exhibits strong fluctuation, owing to the fiercely rising bubbles and gas stream. An important parameter to indicate the intensity of particle fluctuating movement is named the granular

temperature θ and defined as [59],

$$\theta = \frac{1}{3}\left(\sigma_z^2 + \sigma_\theta^2 + \sigma_r^2\right) \tag{2}$$

and

$$\sigma_i^2 = \frac{1}{N}\sum_{i=1}^{N}(v_i - v_m) \qquad i = z, \theta, r \tag{3}$$

where σ_i^2 is the variance of particle velocity, N the total number of samples, v_i the particle velocity in the i direction, v_m the mean of v_i, and z, θ, r stand for the axial, tangential and radial directions, respectively. Cody et al. [60, 61] developed an acoustic shot noise (ASN) technique to estimate the granular temperature using an accelerometer. The particle velocity was determined from the acceleration power spectrum in combination with a wall-transfer function, which was obtained through a series of hammer-impact-excitation experiments. Based on the fact that the particle impacts on the wall generate both acceleration and AE signals, Wang et al. [56] further proposed a semi-empirical formula to describe the relationship between granular temperature and AE energy (represented by the amplitude of AE signal). It was found that the granular temperature varied proportionally to the AE energy, and both were suitable for the indication of solids flow pattern and flow regime transition in a fluidized bed [56]. Furthermore, accelerometers were used on liquid-containing fluidized beds to characterize the bed fluidity and detect the occurrence of particle agglomerate [52, 62].

3.2.2. Characterization of bulk and bubble dynamics

Apart from the characterization of particle-related hydrodynamic properties,

accelerometers can provide information about the bulk and bubble dynamics in a fluidized bed. Unlike the conventional acceleration measurement, de Martin et al. [58] focused on the acceleration signals at the frequencies lower than 20 Hz, since most of the bulk and bubble behaviours occur at relatively low frequencies. Hilbert transform was employed to recover the envelop processes and to extract the low-frequency information from the original signals. Based on cross-correlation analysis between the envelopes and pressure signals, the mechanical vibration and pressure fluctuation were proven to be related processes. By further comparing the Kolmogorov entropy and power spectral density (PSD) of the envelopes and pressure signals, it was shown that the fluidization regime transitions were determined through the acceleration measurement. A hypothesis was therefore proposed that the conventional pressure transmitters could be replaced with accelerometers for on-line monitoring and dynamic diagnosis [63]. In fact, the acceleration signals can be considered as an extension or shift of the pressure fluctuation into the higher-frequency regions [64]. Naturally, the low-frequency flow information should be encoded in the envelopes of the acceleration signals, which are directly related to the pressure signals distributed at 2~8 Hz. From a theoretical point of view, Briongos et al. [65] proposed a model to account for the interaction between the acoustic pressure field and vessel response, revealing a close relationship between the pressure fluctuation and vibration signals. It was also shown that the envelope time series reflect the flow-dynamic forces, while the acceleration signals represented the dynamical response of structures. By analysing the acceleration signals through statistical methods, wavelet transform and

Fourier transform, the fluidization regime transition and the formation of bubbles and clusters were also characterized [66, 67]. However, such analysis leads to a conclusion that the characteristic vibration frequency of bubble motion is in the range of 1000~3000 Hz, which is much higher than that obtained using the low-frequency accelerometer [63] and pressure fluctuation method [68].

Since the particle-related hydrodynamic information is mainly embedded in the high-frequency AE signals, accelerometers are more suitable for the characterization of bulk and bubble dynamics. Although an accelerometer is an applicable alternative to a pressure transmitter, no significant advantage or extra information can be provided until now. Some of the low-frequency information even cannot be recovered from the acceleration envelopes, due to the poor signal emission and measurement construction [63]. However, accelerometers are still promising non-intrusive sensors with similar advantages of AE sensors (Section 3.1.2).

4. Visualization methods

Visualization is an intuitive and straightforward way to characterize the gas-solid flow field, which can provide extensive information about the bubble properties, voidage distribution as well as particle motion. If the observed vessel is of a good optical access and the volume fraction of the dispersed phase is low, a direct photographic technique can be applied. Otherwise, alternative methods such as radiography, nuclear magnetic resonance imaging (NMRI) and tomography, may have to be utilized to visualize the flow inside the vessel.

4.1. Photographic technique

The charge coupled device (CCD) camera is the most commonly used photographic device for investigating the bubble motion and solids flow in fluidized beds [69-72]. A typical schematic diagram of the CCD photography measurement setup is shown in Fig. 5 [73]. The light coming from a Nd:YAG pulsed laser is shaped into a sheet by two cylindrical lenses L1 and L2 to illuminate a plane through a transparent window on the bed. A telecentric lens is used to image the illuminated plane onto the CCD sensor. The optical axis of the imaging system is perpendicular to the laser sheet. It is noteworthy that some CCD imaging systems employ a spot light or a strobe light instead of the laser-sheet for illumination [71, 74]. High-quality images were obtained by carefully adjusting the camera (focus) and selecting the laser intensity for different operation conditions. By processing the recorded images, the bubble dynamic behaviours and particle agglomeration were characterized [73]. However, the solids velocity field is difficult to resolve due to limited spatial resolution of the camera. Particle Image Velocimetry (PIV) in combination with CCD photography is therefore required to present the solids flow at a particle level. We will discuss this separately in Section 4.2.
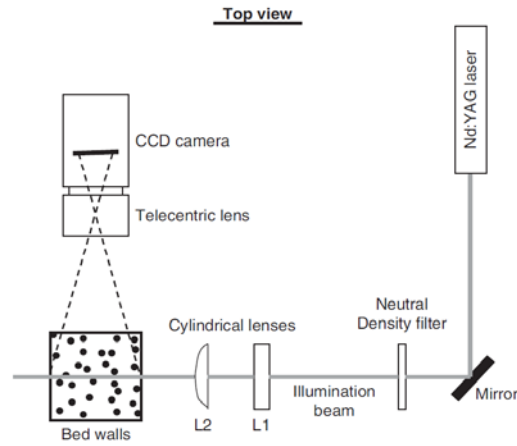
Fig. 5. CCD photography measurement system [73]

4.1.1. Characterization of bubble dynamics

CCD photography in combination with digital image analysis were employed to acquire the bubble dynamic information, including the position, dimension, hold-up, velocity and bubble splitting occurrence [71, 74, 75]. The original images were processed through thresholding, indexing, filtering of false bubbles and peripheral voids as well as property recording [71]. Each image was treated through these steps individually. If the field of camera view is smaller than the investigated section, a calibration method is required to reject the split bubbles [74]. Busciglio et al. [71] introduced two approaches to measure the bubble velocity, named the Eulerian velocimetry and Lagrangian velocimetry, respectively. The Eulerian method is based on the cross-correlation of bubble positions between the pairs of subsequent images. A dominant correlation peak is shown in the background of noise peaks, with the peak location corresponding to the average bubble displacement. The bubble velocity is then obtained from the most likely displacement vector in conjunction with the time

27

delay between two images. In the Lagrangian approach, each bubble is numbered in the first frame and tracked in different frames. A crucial step is to locate a bubble in the subsequent frame with a displacement physically consistent and to assign the same number of the bubble in the first frame. If more than one bubble meet this condition, the same number of the bubble in the first frame will be assigned to the one in the second frame which exhibits a minimum distance from the bubble in the first frame. Once the rising bubbles are indexed, it is possible to measure other local properties of the bubbles as well as their evolution with time.

4.1.2. Characterization of particle clusters and agglomerate

In a fluidized bed, particle clusters and agglomerate are defined as regions with higher solids concentration relative to the mean solids concentration, which are formed by a large number of particles assembling [76]. Such particle groups move as a whole without obvious internal slip motion. According to the classification proposed by Horio and Clift [77], the agglomerate is generated by particles joining together owing to the inter-particle forces, while the clusters are formed due to the hydrodynamic effects. However, the term *agglomerate* is sometimes referred to as *cluster*, although the clusters showing reversible conversion into individual particles could be precursors of the particle agglomerate. As a potential risk for the normal operation of an industrial fluidized bed, particle agglomeration can be considered as an early warning of the fluidization fault occurrence [78]. The agglomerate can be caused by inter-particle cohesive force [73, 79], electrostatic effects [25], liquid

addition [62] as well as high temperature [78]. By using CCD photography and image processing techniques, the size and shape of agglomerate in a fluidized bed were characterized [73]. Firstly, a thresholding method was applied to convert all the 'aggregates' to red color on an image. Then with the increase of threshold index, the background noise was gradually removed. By carefully comparing the thresholding image with the original one, a final image was confirmed and the agglomerate properties were determined. However, each image was required to be treated individually due to the different levels of background noise, and the determination of threshold value is primarily based on experience, making the image processing time-consuming and less reliable. Moreover, the particle agglomerate is defined through the observation of original images, which bring subjective influences on the measurement results and makes this technique unsuitable for the real-time monitoring of agglomerate formation.

Particle clusters commonly exist in circulating fluidized beds (CFBs). They are mesoscale heterogeneous flow structures and continuously formed and broken due to the interactions with gas stream [80]. By using a video camera and a multiple laser-sheet technique, Horio and Clift [77] obtained the shape, size and velocity distribution of clusters in the dilute phase transportation regime. Chew et al. [81] employed a high-speed video camera to characterize the particle clusters in a dilute riser. The area percent occupied by clusters were obtained from the images and the duration and frequency of clusters were calculated from the plot of area percent versus time.

The photographic technique, which provides an intuitive way to probe the fluidization behaviours, has been widely used for the visualization and characterization of flow structures. The hydrodynamic information obtained from the image analysis is also suitable for validation of computational models. However, the requirement of transparent walls or access windows significantly limits the application of the technique to the opaque industrial beds. Besides, in a 3D bed, images of the central region are blurred by the particles near the wall, resulting in difficulties for the identification of flow structures. This may be the reason why the cluster dimensions measured by different researchers exhibit obvious discrepancies [77, 82, 83]. Moreover, the reliability of image processing (such as the threshold setting) depends on the subjective judgements of the researchers to some extent. Despite these drawbacks, the photographic technique is still a promising approach to the on-line measurement and monitoring of fluidization parameters, as long as the image processing techniques are improved.

4.2. Particle image velocimetry

4.2.1. Measurement of solids velocity field

Particle image velocimetry (PIV) is a well-known non-intrusive technique for measuring the solids flow field in a fluidized bed [84-89]. Although the configuration of PIV systems varies in different applications, it mainly consists of a CCD camera, a light source and a computer with image processing software, as shown in Fig. 6. Besides, an electrical motor with a rotating transparency [88] or a PIV controller [89]

can also be included in the system. The rotating transparency is used to determine the direction of particle velocity by analysing the order of the colours in a streak image, as displayed in Fig. 6(b). A streak records the distance that a particle travels in a given time interval determined by the camera. The instantaneous velocity components of an individual particle are therefore calculated from [85],

$$c_r \ or \ c_\theta = (L/t)cos\alpha \qquad (4)$$

$$c_z = (L/t)sin\alpha \qquad (5)$$

where L represents the streak length, α the angle between the streak and the horizontal direction, t the inverse of the camera shutter speed, c_r, c_θ and c_z the radial, tangential and vertical velocity components of a particle, respectively. In spite of the simple sensing principle, the PIV relying on the streak observation requires tedious manual analysis and is therefore limited to the measurement of the dilute flow in quasi-2D beds.
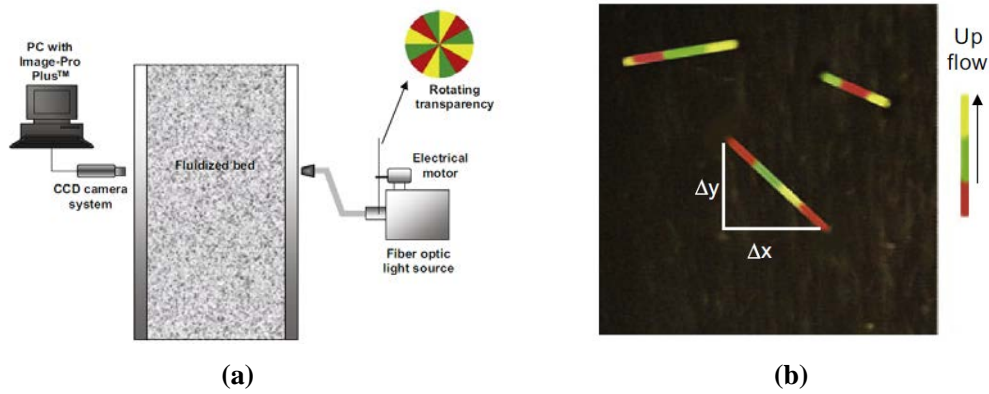

Fig. 6. PIV system, (a) sensing arrangement, (b) a typical streak image captured by the CCD camera [88]

For the dense-phase flow, an alternative PIV approach is to measure the particle

velocity without the identification of streaks [86, 89]. In this approach, a recorded image is divided into different interrogation areas, and the cross-correlation analysis is implemented on the two consecutive images to obtain the volume-averaged particle displacement S_p. In combination with the time interval Δt between the two images, the average particle velocity v_p in each interrogation area is determined by,

$$v_p(x,t) = \frac{S_p}{M\Delta t} \tag{6}$$

where *M* represents the magnification of the image. However, the exact number of particles in each interrogation zone cannot be determined through the PIV software automatically. A modification is hence required to correct the high-velocity regions with a low particle concentration, when measuring the velocity field of the emulsion phase in a fluidized bed. Laverman et al. [86] used an image-analysis based phase separation technique to distinguish the bubbles from emulsion phase. If the pixel intensity on an image is lower than a threshold value, the pixel area is assigned to the bubble phase, otherwise, to the emulsion phase. Yet, the disadvantages of this correction method are the usage of a prescribed threshold value and the characterization of solids fraction by merely using pixel intensity. In addition, the local variation of solids fraction cannot be accounted for due to the 'binary' approach that every pixel is set either to '0' (for the bubble phase) or to '1' (for the emulsion phase) [90]. van Buijtenen et al. [90] and de Jong et al. [91] developed digital image analysis methods to translate the apparent 2D solids volume fraction to true 3D data, using the artificial images of solids distribution obtained from Discrete Element Model (DEM) and Discrete Particle Model (DPM) simulations. In combination with

the PIV solids velocity field, the internal solids flux profiles in the spout and bubbling fluidized beds were obtained, respectively.

4.2.2. Characterization of particle stress and Reynolds stress

The particle velocity data measured by a kinetic theory based PIV system has shown that two kinds of turbulence (or named the fluctuation) exist in a gas-solid fluidized bed [92, 93]. One is the random oscillation at an individual-particle scale, represented by the so-called laminar particle stress or the laminar granular temperature. The other is the turbulence caused by the motion of clusters/bubbles and is characterized by the Reynolds stress or the turbulent granular temperature. The laminar particle stress is defined directly from the instantaneous particle fluctuation velocity in the axial, radial or tangential direction, which is obtained from the streak properties in each frame of the PIV images. The Reynolds stress is computed based on the hydrodynamic particle fluctuation velocity in the axial, radial or tangential direction, which is the average of the instantaneous particle velocities in each frame of the PIV images. Correspondingly, the laminar granular temperature is expressed as the average of the laminar particle normal stresses in all three directions, while the turbulent granular temperature is determined by the average of the Reynolds stresses in the three directions [88]. More detailed definitions about the two granular temperature can be found in Kashyap's Ph.D. Thesis [94]. Moreover, the distribution of granular temperature is an indication of the flow regime and solids mixing pattern in a fluidized bed.

4.2.3. Characterization of solids dispersion coefficients

Solids dispersion coefficient is an important parameter to describe the solids mixing behaviours and varies by at least five orders of magnitude, mainly due to the differences in the system geometries, operation conditions, measurement techniques and even the definitions of dispersion coefficient in different work [95, 96]. The PIV measured particle velocity data can also be used to calculate the solids dispersion coefficients through an autocorrelation method. Corresponding to the solids mixing at the particle scale and cluster/bubble scale, the laminar and turbulent dispersion coefficients are respectively defined as [96],

$$D_{i(laminar)} = \overline{C_\iota C_\iota} T_L \tag{7}$$

$$D_{i(turbulent)} = \overline{v'_\iota v'_\iota} T_L \tag{8}$$

where $D_{i(\text{laminar})}$ is the laminar dispersion coefficient in the i direction, $D_{i(\text{turbulent})}$ the turbulent dispersion coefficient in the i direction, $\overline{C_\iota C_\iota}$ and $\overline{v'_\iota v'_\iota}$ the mean squares of the instantaneous particle fluctuation velocity and the hydrodynamic particle fluctuation velocity, respectively, and T_L the Lagrangian integral time scale for the particle or cluster motion. T_L is defined as,

$$T_L = \int_0^\infty R_L(i, \tau) d\tau = \int_0^\infty \overline{\left(v'(t) v'(t+\tau) \sqrt{v'^2} \right)} d\tau \tag{9}$$

where $R_L(i, \tau)$ is the autocorrelation coefficient for the turbulent dispersion coefficient, τ the frame rate, $v'(t)$ the time-dependent Lagrangian hydrodynamic fluctuation velocity and t the time of frame occurrence.

Attributed to the capability of offering important information about the velocity field, turbulence parameters and dispersion coefficients of solids phase, PIV has

emerged as a desirable non-intrusive tool for characterizing the flow structure evolution and verifying the computational models. However, this technique suffers from some drawbacks. Firstly, an image recorded by a CCD camera requires sophisticated processing, which may lead to measurement delay and difficulties for on-line monitoring. Secondly, a large number of images should be analyzed to acquire a time-averaged flow map, resulting in considerable computational cost. Thirdly, PIV is unsuitable for the 3D dense-phase fluidized beds with strong particle backmixing, since the image quality of the central regions strongly depends on the particle curtains near the walls. More importantly, PIV only allows the measurement on transparent fluidized beds or those with optical access windows. Its applications in the opaque industrial beds, especially those operated at high pressures and temperatures, are hence very limited.

4.3. Radiographic techniques

Radiography, an act of obtaining the shadow images of an object by penetrating through it with radiation such as X-rays and gamma-rays, has been used to visualize opaque multiphase reactors [97]. Owing to the higher spatial resolution and smaller size of the X-ray source, X-ray radiography is preferred in practical applications compared to the gamma-ray approach. Considering the radiation beams (either X-rays or gamma-rays) emitted from a source and traversing a medium, the ray energy attenuation obeys the Beer-Lambert law [98-100], which is expressed as,

$$I = I_0 exp\left[-\left(\frac{\mu}{\rho}\right)\rho l\right] \tag{10}$$

where I represents the ray energy recorded by a detector, I_0 the energy of the radiation source, μ/ρ the mass absorption coefficient of the medium, ρ the medium density and l the path length through the medium. According to the fact that gas and particles have different absorption coefficients for the rays in a gas-solid mixture, the magnitude of the transmitted rays is expressed as a linear function of the volume fraction of the gas and solids phases [97],

$$I = I_0 exp\big[-\big((1-\varepsilon)\mu_1 + \varepsilon\mu_2\big)l\big] \tag{11}$$

where μ_1 and μ_2 are the linear absorption coefficients of the gas and solid phases, respectively, ε the solids volume fraction, which can be determined from this formula.

The radiographic techniques applied on gas-solid fluidized beds are basically classified as X-ray radiography, X-ray computed tomography and gamma-ray computed tomography. We will introduce the sensing principles and applications of these techniques in the following sections. In order to facilitate the comparisons, the tomography techniques will be discussed separately in Section 4.4. Although the gamma-ray densitometry is not a visualization method, it is based on radiation absorption principle and is thus included in Section 4.3.

4.3.1. X-ray radiography

Based on the attenuation characteristics of the X-ray beams penetrating through a medium, the 2D projections of a 3D object can be recorded by an X-ray imaging device, when the object is placed between an X-ray source and a detector. Since X-rays can expose a photographic film, the traditional radiography was implemented

with a film-based detector and the 'shadow pictures' of an object could be acquired. Currently, the digital detectors, which produce images through the electronic capture of the X-ray intensity, are used more commonly than the film-based detectors. The major advantages of the digital radiography over the film one are the higher speed of image acquisition as well as the flexibility in manipulating and storing images. If the measured object is gas-solid flow, the response and recording speeds of the detection and imaging devices must be fast enough, otherwise the projection images will be blurry due to the complex movement of different phases. Such radiography technique used in the dynamic processes is also referred to as the fluoroscopic imaging. The original definition of 'fluoroscopy' is to observe an X-ray image on a fluorescent screen in real time [97, 101].

X-ray radiography has been used for a long time to probe the interior of a fluidized bed and to enable direct observation of the bubble motion [3, 99, 102, 103]. An example of the measurement setup is shown in Fig. 7, which consists of an X-ray tube, an X-ray detector, an image intensifier and a data acquisition computer [3]. The continuous X-rays generated by the X-ray tube penetrate through the bed before reaching the detector, which converts the X-ray photons into electrical signals. The image intensifier then enhances the electrical signals and transforms them into a digital grayscale image. The images were captured at a rate of 30 frames/s by the data acquisition computer [3]. In order to identify the bubble boundaries, a global threshold was firstly applied to binarize the grayscale images. Bubbles were then tracked in a MATLAB program frame by frame and the information about the bubble
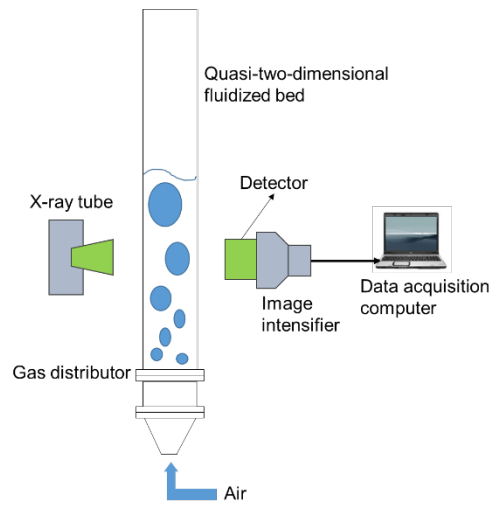
dimensions and velocity was obtained.

Fig. 7. X-ray radiography system [3]

Although X-ray radiography is a useful tool for visualizing the bubble distribution and motion, its spatial resolution is insufficient for the identification of particle motion. In addition, the cost of an X-ray apparatus is higher than other sensors (e.g. electrostatic sensor, AE sensor and accelerometer), and the image processing speed is slow. Moreover, special protections are required for X-ray radiography to comply health and safety regulations.

4.3.2. Gamma-ray densitometry

Gamma-ray densitometry is a non-intrusive and non-destructive technique that has been applied to study the gas-solid flow hydrodynamics for more than fifty years. As an electromagnetic radiation similar to X-rays, gamma radiation acts as a by-product of the natural decay of some radionuclides. Owing to the sufficiently high ray energy ranging from 10 keV to 10 MeV, gamma rays can penetrate the media

impermeable to X-rays [104]. By using a gamma-ray densitometer to record the absorption of the gamma-rays passing through a gas-solid fluidized bed, the solids volume fraction can be measured. Fig. 8 shows a typical measurement setup of a gamma-ray densitometer on a downcomer [105]. A radiation source and a detector are aligned on a carriage that is moved around the downcomer to scan different chords through the cross-section of the column. The radiation source is [46]Sc and collimated by a lead cylinder with the wall thickness of 12 mm and aperture of 4 mm. The intensity of the emitted gamma-ray photons is detected by a NaI (TI) scintillation detector, which is connected to a photomultiplier tube, a pre-amplifier, a timing filter amplifier, a scalar and a discriminator (not shown in Fig. 8). The detector output is finally captured by a data acquisition system. Before the measurement, calibrations were carried out by collecting the ray intensity data from the empty downcomer and the one filled with static particles, respectively. By this means, the absorption properties of the downcomer, air and packed particles were characterized.
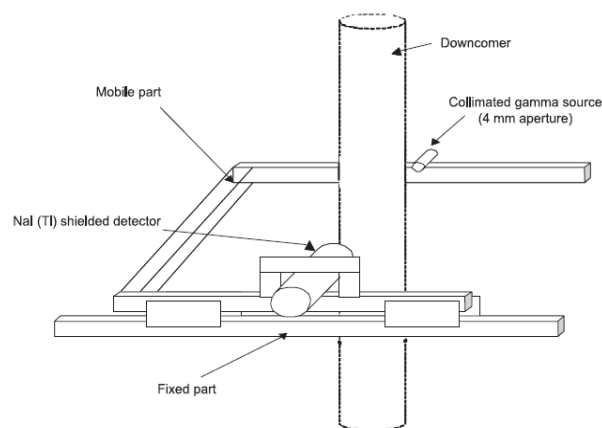

Fig. 8. Gamma-ray densitometry system [105]

Huilin et al. [100] measured the local instantaneous porosities in a riser using a gamma-ray densitometer. The signal series of porosity fluctuation was further processed by a deterministic chaos analysis method. It was found that the attractor dimension was basically consistent with that of the pressure fluctuation signal. Bhusarapu et al. [105] estimated the solids mass flux in a CFB loop through a gamma-ray densitometer in combination with the radioactive particle tracking (RPT) technique. The former was used to measure the cross-sectional averaged solids hold-up while the latter was to obtain the solids velocity from the time of flight measurement of the radioactive tracer traversing the axial distance between the detectors. The deviation between the estimated solids mass flux and that obtained by a timing and weighing method was within 4%. Jiradilok et al. [106] computed the viscosity of nanoparticles based on the solids volume fraction measured by a densitometer. The predicted value was close to that estimated from the kinetic theory. Kashyap et al. [88, 107] characterized the solids slugging and flow patterns in a riser under high and low solids fluxes, respectively. Gidaspow & Driscoll [108] determined the speed of a compression wave in a fluidized bed, based on principle that a small dip followed by an upward shift in the gamma-ray voltage signal indicated the passing of a compression wave.

Gamma-ray densitometry is a non-intrusive, relatively inexpensive, reliable and portable measurement technique applicable to gas-solid flow systems. It is available for the one-shot or traverse measurements and the single- or multi-beam configurations as well as the single- or dual-energy sources [109]. However,

40

calibrations are required prior to the measurement under the desired operation conditions. Besides, this technique only allows the measurement of line-averaged solids volume fraction instead of the local value. With the increase of the thickness or density of the column wall, the intensity of the gamma-ray source should be increased correspondingly, which will compromise the instrument portability and entail more stringent requirement for radiation protection.

4.4. Tomographic techniques

Tomography is the representation of a 3D structure as a series of 2D images generated from the parallel sections of the structure. A *tomogram* is a single sectional image and a *tomograph* is a device used in the preparation of a *tomographic dataset* (a series of tomograms). The tomographic dataset can be studied directly or used as a basis for 3D reconstruction of the original structure [110]. In the medical field, tomography largely relies on the use of high energy electromagnetic radiation such as X-rays and gamma-rays. While in the engineering field, there are also other forms of tomography, including those based on capacitance, resistance, ultrasound and even visible light [111]. The tomographic techniques can be applied to gas-solid fluidized beds for the measurement of phase distribution, through recording and reconstructing the signals of certain physical properties over the cross-sections of the beds. In this section, we will discuss the tomographic techniques, including the electrical capacitance tomography (ECT), X-ray computed tomography (X-ray CT), gamma-ray computed tomography (gamma-ray CT) and nuclear magnetic resonance imaging

(NMRI).

4.4.1. Electrical capacitance tomography

Electrical capacitance tomography (ECT) allows the measurement of capacitance changes resulted from the variations of concentration and/or distribution of dielectric materials by employing a multi-electrode ECT sensor, which consists of one (2D tomography) set (plane) or several (3D tomography and ECT-based flowmeter) sets (planes) of electrodes mounted on the side surface of the measured fluidized bed [112]. The electrodes are excited consecutively by direct current (DC) or alternating current (AC) voltage sources and the capacitances between the excited electrode and the remaining ones are measured. In combination with a reconstruction algorithm, the cross-sectional or 3D images of solids concentration distribution in a fluidized bed are obtained. There are two types of reconstruction methods known as the non-iterative algorithms (e.g. linear back-projection (LBP), singular value decomposition, Tikhonov regularization as well as multiple linear regression and regularization) and iterative algorithms (e.g. Newton–Raphson, iterative Tikhonov, steepest descent, Landweber iteration, conjugate gradient, algebraic reconstruction, simultaneous iterative reconstruction as well as model-based reconstruction), which have been reviewed comprehensively by Yang & Peng [113]. There're also new algorithms developed recently, e.g. the total variation iterative soft thresholding method in which the sharp transition of permittivity distribution between the bubble phase and solids phase is taken into account [114]. With the development of sensing and reconstruction

techniques, the electrical capacitance volume tomography (ECVT) technique has been proposed to allow real 3D imaging of gas-solid flow, whereas pseudo 3D images from the traditional ECT are obtained by stacking 2D images for interpolation [115-118]. ECVT is realized through a geometrically configured 3D sensor and additional objective functions used in the optimization scheme for reconstruction. Sensor design is especially important for ECVT and a desired sensor is expected to provide equal distributions of electric fields in all the three directions [119].

Fig. 9 shows an ECT measurement system applied on a gas-solid fluidized bed [119]. For N electrodes, the total number of independent measurements is $N(N-1)/2$. The image acquisition rate provided by this measurement system was up to 100 frames/s [119]. It is commonly assumed that the increase of electrode number would improve the image quality, however, limited new information and improvement of image quality were obtained when the electrode number exceeded 12 [120]. Besides, the image quality also depends on the reconstruction algorithm. Until now, extensive work has been conducted on the characterization of fluidization behaviours using ECT, such as the flow structures in different fluidization regimes [121, 122], inhomogeneity in a turbulent bed [123], choking phenomena [124-126], dense-phase transportation behaviours [127] as well as jet characteristics in a fluidized bed [128].
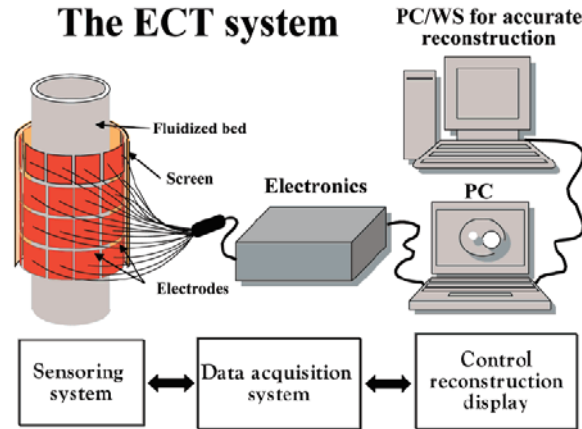
Fig. 9. ECT measurement system [119]

Apart from imaging, the solids concentration fluctuation signals obtained through ECT can be processed to characterize different flow behaviours. The commonly employed data analysis methods include time domain analysis (e.g. standard deviation, skewness, excess kurtosis and auto-correlation) and frequency domain analysis (e.g. power spectrum and wavelet analysis). In combination with the reconstructed images, both qualitative and quantitative information about the flow field can be acquired. For instance, the geometry and distribution of bubbles are directly observed from the reconstructed images, and the information about bubble velocity and frequency is extracted from both the images and the solids concentration fluctuation signals [129, 130]. Other information about the particle residence time distribution (RTD) [131], flow structures [132], transition velocities between flow regimes [129, 133], and fluidization quality [134] can also be characterized through the analysis of solids concentration fluctuation signals.

Significant progress has been made in developing the ECT techniques for gas-solid fluidization measurement over the last two decades. The major advantages

of ECT are the fast imaging speed, low cost and suitability for high temperature and pressure conditions [135]. ECT is also a tool for verifying CFD models [136]. However, ECT is a typical 'soft-field' technique. The variation of the capacitance in one location will change the recorded field through the whole domain, making the signal reconstruction sensitive to errors and noises and resulting in ambiguous solutions. In addition, the quality of the reconstructed images is limited by the number of independent electrodes and is highly sensitive to the reconstruction algorithm. It is also difficult to reconstruct the images of the central region in a fluidized bed due to the low sensitivity of the ECT sensor, especially when there're particles in the vicinity of the wall or when the bed diameter is enlarged. Moreover, electrostatics in the fluidized bed can result in measurement inaccuracy and even malfunction of some ECT systems [135]. Due to these drawbacks, the applications of ECT to industrial fluidized beds are still very limited.

4.4.2. X-ray computed tomography

Although X-ray CT and gamma-ray CT differ in radiation sources, namely the X-ray tube and encapsulated gamma-ray source, respectively, they follow a common sensing principle. A narrow radiation beam that traverses a straight path through an object attenuates primarily by absorption and to a less extent by scattering. Supposing the object is divided into different elements, a CT technique is to determine the attenuation degree of the beam in each element, and to display this information in the form of images [111]. According to the Beer-Lambert's law (Eq.(10) and Eq.(11)),

solids volume fraction is obtained from the radiation intensity signal. For a gas-solid fluidized bed, a cross-sectional image showing the internal structures are reconstructed from multiple projection images. The X-ray CT system mainly consists of two parts. Firstly, physical instruments are used to obtain the integral values of a local variable along certain paths, as schematically shown in Fig. 10 [98]. An X-ray tube emitting a fan-shaped beam and a linear detector are mounted on a ring, which can be rotated with the support of a step-by-step motor. Since the fan-shaped beam covers a whole cross-section of the measured riser, the ray intensity distribution on the entire plane can be determined through one single measurement. By rotating the X-ray tube and detector, views from different angles are recorded for further data reconstruction. Secondly, reconstruction algorithms are adopted for the computation of local solids volume fraction on the cross-section [98, 137].
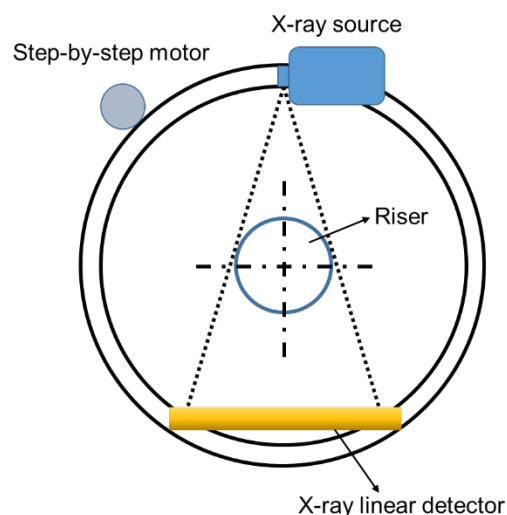

Fig. 10. X-ray CT system [98]

Owing to the recent advances on the single-beam ultrafast X-ray CT and

multiple-beam fast X-ray CT, it is possible to characterize the cross-sectional flow behaviours in a fluidized bed with high spatial and temporal resolutions, even at high superficial gas velocities [138-140]. The ultrafast X-ray CT is based on a 'scanned electron beam' principle. A typical measurement setup is shown in Fig. 11. The electron beam emitted from an electron gun rapidly sweeps across the circular object, and a moving X-ray source is hence produced. A fixed detector ring synchronously captures the intensity of the X-rays passing the measured object. Based on the resulted radiographic projections, the non-superimposed cross-sectional density distribution is reconstructed. Without the mechanically moving parts as those in the conventional X-ray CT system, the speed of the ultrafast X-ray CT can reach up to 10000 frame/s. Verma et al. [139] applied the ultrafast X-ray CT to bubble property characterization. Bubble coalescence and breakup were observed in the reconstructed cross-sectional image sequences, and the bubble velocity was determined through cross-correlation of images from dual horizontal planes. Pseudo 3D bubble shapes were also reconstructed from the pixel intensity variations with time. However, the vertical axis represented time instead of a length scale, as the bubbles with different sizes had different velocities. In addition, it is possible for the ultrafast X-ray CT to identify particulate structures and even track particle movement in a fluidized bed, as its spatial resolution can be down to 1 mm if the contrast of the involved materials is sufficiently high [138].
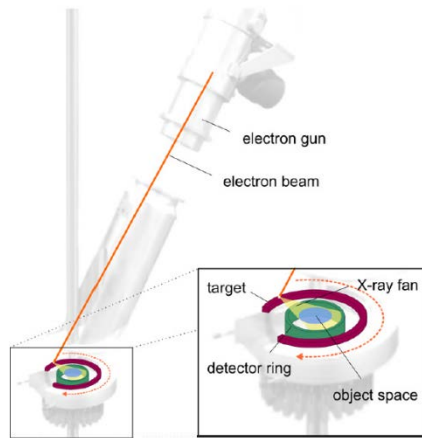
Fig. 11. Ultrafast X-ray CT system [138]

Fig. 12 shows the top and side views of a typical measurement setup of multiple-beam fast X-ray CT [140]. Three X-ray sources are placed around the fluidized bed column. Opposite of each source is a detector array consisting of the up and bottom rows with 32 detectors respectively, which creates 64 measurement lines through the column for each source. Such a sensing arrangement also results in two separate measurement planes. All the 192 detectors were used to record images at a frequency of 2500 Hz [140]. This technique provided information about the mean solids holdup, solids holdup profile, void dimension and void velocity in different fluidization regimes. Pseudo 3D structures of voids/bubbles were also reconstructed.
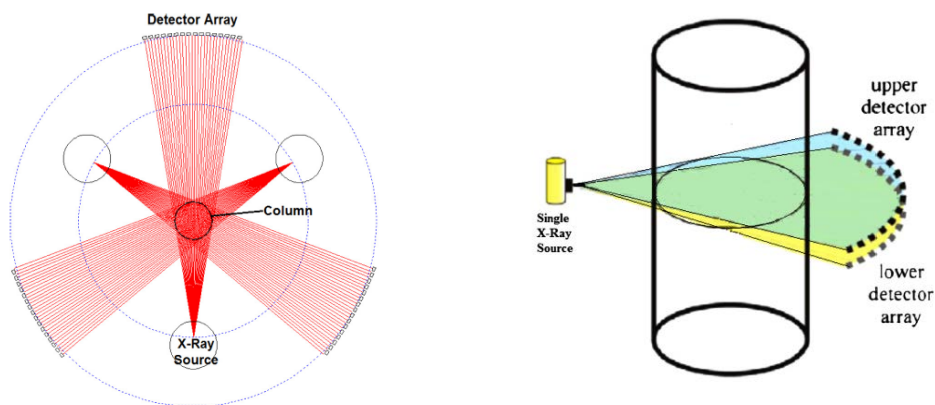
Fig. 12. Multiple-beam fast X-ray CT system, (a) Top view of the three sources and

detector arrays, (b) Side view of the single up-and-bottom detector array [140]

X-ray CT is the safest 'hard-field' measurement technique, with a higher spatial resolution than gamma-ray CT [141]. Since the field lines of X-ray attenuation remain straight and are not influenced by the property changes outside the line-of-sight, the image reconstruction is easier than that for the 'soft-field' techniques such as ECT [97]. Besides, X-ray CT is insensitive to electrostatic charge build-up in gas-solid fluidized beds [97]. The larger measurement plane/volume and the capability of withstanding high temperature also make X-ray CT more suitable for industrial applications. However, the conventional X-ray CT is only valid for the measurement of time-averaged parameters due to the slow data acquisition speed and the relatively low temporal resolution. Recent advances on the single-beam ultrafast and multiple-beam fast X-ray CT techniques allow time-resolved measurement on fluidized beds. The ultrafast X-ray CT has advantages of no moving parts, fast scanning capability, high imaging speed and high versatility. However, the contrast of the materials under test needs to be sufficiently high and the particle size should be large enough compared to the bed diameter. In addition, the data processing and image reconstruction for the ultrafast and fast X-ray CT could be cumbersome. Other drawbacks of X-ray CT are the complexity of operation, high cost, large space occupied and compliance for health and safety regulations.

4.4.3. Gamma-ray computed tomography

In a gamma-ray CT system, the gamma-rays emitting photons through the β^- decay process can penetrate through the object under test. The radiation is measured by scintillation detectors placed on the opposite side of the radiation source, which is commonly made of radioisotopes such as ^{137}Cs, ^{241}Am and ^{153}Gd [102]. Since the sensing principles and applications of gamma-ray CT and X-ray CT have been comprehensively reviewed by Chaouki et al. [111], in this paper we just briefly introduce a typical gamma-ray CT system applied on a laboratory-scale fluidized bed dryer, as shown in Fig. 13 [142]. The measurement system is composed of a 1 mCi ^{137}Cs gamma source, sodium iodide (NaI) with thallium (Tl) activated scintillation detectors, a photo multiplier tube, a preamplifier, a multi-channel analyzer and a data acquisition system. Fan-shaped beam is employed and the grid scanning is implemented at different axial locations. For each source position, 7 detectors are equally placed at an interval of 8° on an arc with 30×10^{-2} m in length. The chordal gas holdup was obtained through each measurement. Patel et al. [142] further applied the gamma-ray CT on an industrial-scale dryer with 1.0 m diameter and 0.5 m^3 capacity. The extent of gas maldistribution related to the fluidization quality was clearly identified from the measured solids holdup profiles. For image reconstruction, Dudukovic et al. [111, 143] found that among the suggested reconstruction algorithms, such as the convolution or filtered back projection, algebraic reconstruction and estimation-maximization (E-M) algorithm, the E-M algorithm yielded the best results.
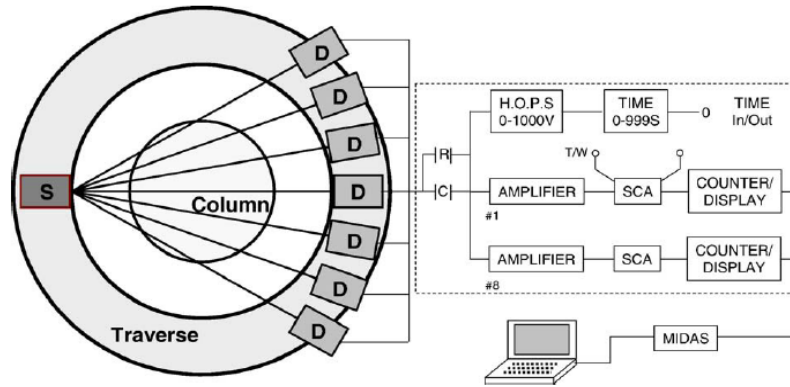
50

Fig. 13. Gamma-ray CT system (S representing the 1 mCi ^{137}Cs gamma-ray source and D representing the NaI(Tl) detector) [142]

Gamma-rays emit photons with higher energy and thus are more penetrative than X-rays. Therefore, gamma-ray CT is more suitable for the measurement of large test sections. However, X-ray CT provides better spatial resolution attributed to the smaller detectors. In addition, the X-ray source emits radiation only when it is powered on and the radiation energy can be controlled by varying the input voltage, which makes X-ray CT safer than gamma-ray CT [102]. Based on these reasons, gamma-ray CT has gained less applications than X-ray CT on the gas-solid systems, especially in recent years. To the best of our knowledge, McCuaig et al. [144] for the first time adopted a single mono-energetic gamma-ray beam generated from a 100 mCi ^{241}Am source and a single NaI (Tl) detector to study the density distribution and flow structures in a fluidized bed. Landeghem et al. [145] then measured the solids concentration profiles in a cold model riser and an industrial riser through gamma-ray CT, respectively. The core-annulus flow structures were found in both risers. Bhusarapu et al. [146] combined gamma-ray CT with the computer automated

radioactive particle tracking (CARPT) technique to develop coherent pictures of the solids flow field in a riser. The time-averaged solids holdup distribution was reconstructed to characterize the flow behaviours under different fluidization regimes.

Gamma-ray CT acts as a 'hard-field' technique similar to X-ray CT, which reduces the influence of the flow field outside the line-of-sight and simplifies image reconstruction. Gamma-ray CT offers phase distribution images and hence solids concentration profiles with a high spatial resolution and is immune to electrostatic disturbances. Due to the stronger penetrability, gamma-ray CT can be applied to some industrial fluidized beds with the dimensions in a few meters. However, depending on the scanner design, the time required for the photon count rates for all the projections ranges from a few minutes to close to an hour. Such a long sensing time is a significant limitation of gamma-ray CT in the measurement of time-evolving flow behaviors, such as bubble motion and evolution [102]. Other disadvantages of gamma-ray CT are similar to those of X-ray CT (Section 4.4.2).

4.4.4. Nuclear magnetic resonance imaging

Nuclear magnetic resonance imaging (NMRI), based on the paramagnetic properties of nuclei, is a non-intrusive technique that allows the measurement of dynamic properties in a granular system. The spin motion of a nucleus is characterized by the spin quantum number I. The nuclei with $I=1/2$ are widely used in NMRI since they can be treated as small magnets during their spin motion. For instance, a hydrogen nucleus has a spin quantum number I of 1/2 while a deuterium

nucleus has *I* of 1. The angular momentum and magnetic dipole moment (proportional to the angular momentum) are associated with the nuclear spin. The proportionality constant relating the angular momentum with magnetic dipole moment is named the gyromagnetic ratio [102]. During the measurement, a constant and homogeneous magnetic field is applied. All nuclei then try to align their moments to this external field. Subsequently, a magnetic field at 90° with the external field is pulsed, which kicks the nuclear magnets out of alignment and causes their precession with the Larmor frequency. Such precession is analogous to the motion of a spinning top under the action of gravity. After the pulse, the spinning nuclei decay towards the aligned situation. The spin amount in a particular point in the space is obtained from the decay, based on which the density of the material under test is estimated. Since different phases have different proton densities (e.g. different hydrogen density), the local phase distribution can therefore be determined. By scanning over a cross-section or a volume, sufficient information is collected for tomographic reconstruction [147]. Yet it is inherently difficult to image solid particles due to their very rapid nuclear spin relaxation properties. A common way to overcome this is to use particles containing the materials with liquid-like relaxation characteristics, such as seeds or porous particles impregnated with liquid [148].

Fig. 14 shows a NMRI system to image the gas jet near the distributor of a fluidized bed [149]. Poppy seeds with 0.5 mm diameter (Geldart B) and 1.2 mm diameter (Geldart D) were used as fluidized particles, due to their high content of oil with the mobile ^{1}H nuclei detectable by NMRI. Experiments were carried out in a 4.7

T (199.7 MHz ^{1}H frequency) magnet equipped with a spectrometer. The actively shielded gradient system allowed the production of a maximum gradient strength of 0.139 T/m. A birdcage radiofrequency coil with an inner diameter of 63 mm was mounted on the bed to excite and detect the ^{1}H nuclei signals.
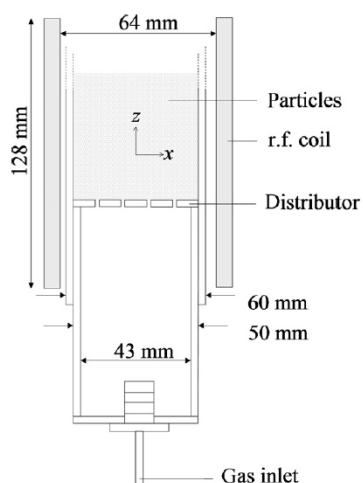
Fig. 14. NMRI system [149]

Salvesberg et al. [150] measured the time-averaged density and particle motion properties in a fluidized bed with an inner diameter of 21 mm, employing the NMR k-space and q-space imaging techniques. Transitions toward the fluidization, bubbling phase and slugging phase were observed from the sudden changes in the density and the root-mean-squared displacement. The effective diffusion coefficients and the particle displacement distribution (or propagators) were also determined. Fennell et al. [151] used the ultra-fast NMRI to study the mixing behaviours of sugar crystals in a fluidized bed by adding a small batch of poppy seeds as tracers. The experiments were implemented on a Perspex tube with an inner diameter of 50 mm. The real-time information (every 12 ms) about the seeds motion was provided with a spatial

resolution of 0.625 mm. The segregation index, representing the degree of mixing, was also calculated from the standard deviation of the normalized intensity of NMR signal. However, the bed materials and tracers are not typical particles used in the normal fluidized beds, and the adoption of ballotini as a distributor is not ideal as well. Muller et al. [152, 153] employed a similar NMRI technique to measure the velocity of bubbles and solids phase, the geometry of bubbles and slugs as well as the bubble coalescence and splitting. By conducting a series of experiments with increasing magnitude of the motion encoding gradients, the spatially resolved maps of granular temperature were obtained [148, 154]. It was confirmed that NMRI mainly allows the measurement of bubble-like granular temperature rather than laminar granular temperature. The hydrodynamic characteristics of gas jet in a fluidized bed was also studied using NMRI, coming to a conclusion that NMRI provided higher-resolution maps than ECVT [149, 155, 156].

Although NMRI has been utilized to characterize some dynamic properties of the solids phase and bubbles, the direct imaging of gas phase is less well studied since the hydrogen nuclear spins in certain particles give high signal-to-noise ratio but convey no direct information about the gas flow [152, 157]. Wang et al. [158] and Pavlin et al. [157] used the laser polarized ^{129}Xe as fluidizing gas to probe the gas exchange rate between the bubbles, emulsion phase and absorbed phase. The gas velocity distribution was also measured. However, such special requirement for the fluidizing gas limits the application of this technique to larger fluidized beds (the bed diameter in their work was only 8 mm).

Until now, advances in NMRI allow the imaging of solids velocity distribution in a fluidized bed with high spatial and temporal resolutions, as well as the measurement of material density and gas dynamic properties. However, NMRI is limited by the requirement for particles containing the MR-sensitive nuclei (typically ^{1}H), by the bore size of magnet, as well as by the need for elimination of metals from the apparatus [156]. In addition, the static magnetic field should be strong enough, which restricts the used permanent magnets to a relatively small size. In spite of the fact that super-conducting magnets can be made stronger and larger, the cost of such NMRI system is considerably high [147].

From the comparison of the aforementioned tomographic techniques (Section 4.4.1~4.4.4), it is known that trade-offs have to be made when imaging measurement is implemented on gas-solid fluidized beds. ECT is applicable to multiphase media with dielectric properties, with major advantages of fast imaging speed, low cost and suitability for high temperature and pressure conditions [135]. In comparison with X-ray/gamma-ray CT, ECT has a poor spatial resolution but a relatively high temporal resolution, and the reconstructed results rely, to some extent, on the number of independent electrodes and the reconstruction algorithm. X-ray/gamma-ray CT has good spatial resolution while low temporal resolution, which makes it most suited for the measurement of time-averaged phase distribution. The development of fast X-ray CT now allows time-resolved imaging of a fluidized bed [159]. In addition, X-ray/gamma-ray CT is not influenced by the property changes outside the line-of-sight and insensitive to the electrostatic phenomena in a fluidized bed, both of

which are problematic for ECT. The drawbacks of X-ray/gamma-ray CT are mainly the complexity of operation, high cost, large space occupied and compliance for health and safety regulations. NMRI provides high spatial and temporal resolution results, but is limited in the particle species and bed size. Therefore, the application of NMRI to gas-solid fluidized beds is still limited compared to that of ECT and X-ray/gamma-ray CT.

4.5. Infrared thermography

In recent years, infrared thermography has emerged as a non-intrusive technique to measure the temperature distribution and heat transfer properties in gas-solid fluidized beds [160-162]. It is based on the principle that an object with the temperature above 0 K emits infrared radiation, which can be detected by an infrared camera. The temperature of the object surface (e.g. particle surface) is then directly determined from the relationship between the temperature and the infrared radiation energy. However, if the particle surfaces are polished, the accuracy of temperature measurement will be influenced by the infrared ray reflection from the surrounding particles. A feasible solution is to coat the particles with a black-body paint to reduce the reflection [163]. For the measurement of solids properties in a fluidized bed, infrared thermography has been used in conjunction with PIV to characterize the coupling relationship between the particle motion and heat transfer [162, 164]. The measurement setup is illustrated in Fig. 15. An infrared camera and a high-speed visual camera are placed in front of a quasi-2D bed. The back and side walls of the

bed are made of aluminium coated from the inside with matt finish black paint to reduce reflection. The aluminium frame is anodized to give the material better adhesion for the paint and glue to attach a sapphire window. The whole frame is also corrosion- and wear-resistant and helps to reduce the charging of particles. A pair of white LED lamps are set at an angle of 45° to the normal of the front wall. Such arrangement also minimises the reflection and shining effects. The infrared camera is installed not fully perpendicularly to the sapphire window to avoid the visibility of a cold spot. The two cameras are connected to a trigger box and then to a computer. The trigger box sends simultaneous pulses to the cameras, ensuring that the two cameras record images synchronously. By this means, the obtained thermographic data are coupled with the concurrent flow hydrodynamic data. Brown and Lattimer [161] also employed an infrared camera to capture the full field views of transient particle temperature distribution in a spouted bed, based on which the distribution rate of the energy stored in particles and the gas-to-particle heat transfer coefficients were obtained.
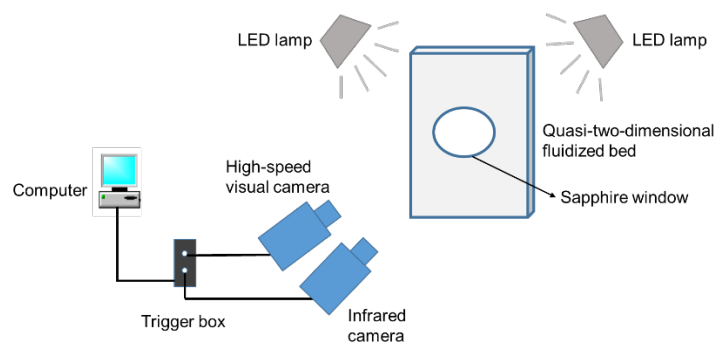
Fig. 15. Measurement setup of an infrared camera in conjunction with a visual camera

[162]

Moreover, infrared thermography allows the measurement of phase distribution in a fluidized bed. By applying an infrared camera to the single-bubble injection experiments, Dang et al. [165] visualized the concentration distribution of CO_2 tracer gas and estimated the gas exchange coefficients from the bubble phase to emulsion phase. The authors then extended the technique to bubbling and turbulent fluidization regimes to quantify the lateral gas dispersion coefficients [166]. An innovative particle tracking technique was developed by Zhong et al. [167, 168] through a combination of a microwave heating apparatus with an infrared camera. A flat-bottom spout bed was made of microwave transparent Plexiglas and placed in a specially designed microwave heater. Polar tracer particles were introduced into the bed and heated by microwave energy. An infrared camera was used to image and record the particle trajectories. This infrared based method provided information about the particle cycling, particle residence time distribution and solids mixing quality. However, it requires a specially designed fluidized bed built inside a microwave heater, which significantly limits the applicability.

Infrared thermography offers a solution to the visualization of phase and temperature distribution with relatively high temporal and spatial resolutions. However, the reflection and absorption of infrared radiation by the bed and particles themselves are important factors that affect the image quality. It is thus required to adopt a surface-polished sapphire window and particles coating with a black-body paint. In an industrial bed (especially the one operated at high pressure), such stringent requirements can hardly be met, primarily because it is difficult to fit an

optical access window on the wall and prevent the window from being contaminated by fine particles. Therefore, thermocouples are still the most common devices for the temperature measurement of the fluid in fluidized beds.

5. Particle tracking methods

Apart from the radiographic and ray tomographic techniques, nuclear radiation can also be utilized to track the particle movement in a multiphase flow system. This allows the measurement of velocity fields of the continuous or dispersed phase in a dense-phase fluidized bed, where the laser based approaches will not work. Currently, there are two different particle tracking methods that employ the nuclear radiation, known as the radioactive particle tracking (RPT) and positron emission particle tracking (PEPT), respectively.

5.1. Radioactive particle tracking

Radioactive particle tracking (RPT) is performed by firstly introducing a radioactive tracer particle emitting gamma radiation into a flow system. The density and size of the tracer match with those of the recirculating phase. The majority of radionuclides adopted in RPT are the β^--emitters produced by neutron capture. These emitters often result in the formation of an excited state in the daughter nuclei, which decay to the ground state by emitting one or several characteristic gamma-rays. These gamma-rays cross the medium in a fluidized bed and interact through the photoelectric absorption and Compton scattering. As the tracer particle moves with the recirculating phase, the gamma-ray intensity is recorded by an array of inorganic

scintillation detectors (generally the thallium-activated alkali halide scintillation crystals) positioned around the bed [102]. While the tracer particle is tracked, the operation condition should be controlled and kept constant for several hours. The instantaneous positions of the tracer are then computed from the intensity signals using an optimized linear regression scheme. The time differentiation of the displacement yields the local velocity of the tracer. Correspondingly, the ensemble-averaged velocity distribution and other turbulence parameters can be obtained by analysing the signals over a period of time [169]. Fig. 16 shows a schematic diagram of the RPT system applied on a gas-solid fluidized bed [170]. The main part of the fluidized bed is a column with an inner diameter of 78 mm and a height of 750 mm. Eight detectors are placed 40~60 mm away from the column wall. The tracer particle was made of scandium oxide, and its density and size were close to those of the fluidized particles (silica sand). The tracer was activated to 300 μCi in a nuclear reactor. Each experiment lasted for at least four hours.
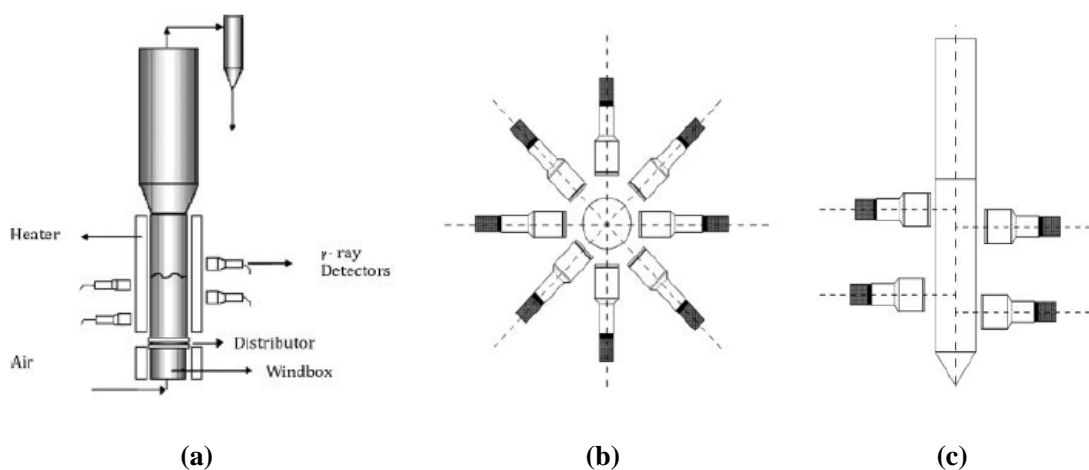

(a) **(b)** **(c)**

Fig. 16. RPT system, (a) sensing arrangement, (b) top view, (c) side view [170]

The sensing principle and applications of RPT have been known for a long time. As early as 1964, Kondukov et al. [171] employed six scintillation detectors to continuously record the tracer particle positions in a fluidized bed. Based on the calibration curves and the recorded signals, the coordinates of the tracer particle were obtained. Lin et al. [172] improved the signal processing scheme by utilizing the signal redundancy to reduce the intrinsic noise level due to the quantized nature of Gamma emission. Hydrodynamic parameters related to the particle motion have been measured through RPT, such as the trajectory, velocity, RTD, diffusivity, cycle frequency, turbulent kinetic energy and Reynolds stress [169, 170, 173-177]. The tracer trajectory was also used to characterize the particle-wall contacting parameters and the friction factor [178-180]. Based on the particle backflow phenomenon in a riser, Bhusarapu et al. [105, 146, 181] measured the solids circulation rate, overall solids flux and turbulent parameter profiles. More dynamic properties were characterized by processing the RPT signals through statistical analysis, non-linear dynamics analysis, symbolic dynamics analysis and data mining [182-184]. Moreover, a multiple radioactive particle tracking (MRPT) technique has been developed to determine the trajectories of multiple tracers in the three dimensions. The MRPT helps reduce the data collection time and image number, as well as improve the image quality [185, 186].

Early extensive work has demonstrated that RPT is suitable for the non-intrusive measurement of solids flow parameters in opaque fluidized beds, on the basis of a

Lagrangian description of particle motion [187]. RPT is also a tool for the validation of CFD models [146]. However, the calibration procedure of RPT is cumbersome since the tracer needs to be positioned at hundreds or even thousands of known locations. The tracking process usually lasts for several hours with the operation condition unchanged, making it time-consuming to obtain the time-averaged properties such as the flow pattern. Moreover, the tracer particles have to be selected or specially made to follow the motion of the recirculating phase. It is also not trivial to set up a RPT apparatus and apply it to a system with irregular moving boundaries. Therefore, the application of RPT on gas-solid fluidized beds seems not as wide as that of the radiation-based visualization techniques.

5.2. Positron emission particle tracking

The positron emission particle tracking (PEPT) technique employs the radionuclide which decays via β^+ decay and emits a positron as a tracer. The positron does not travel far but annihilates rapidly with an electron in its vicinity, producing a pair of 511 keV gamma-rays emitted almost back-to-back [188]. By detecting the two gamma-rays with two position-sensitive detectors, it is known that the positron-emitting particle should be somewhere on the line connecting the two gamma-rays. After detecting the positions of more gamma-ray pairs during a time interval in a similar way, the location of the tracer particle is determined by the displacing crossings of these lines [147, 189]. However, gamma-rays can be corrupted in the practical measurement, which makes the lines connecting the two ends of the

counter-propagating gamma-rays may not pass the tracer source. The actual position of the tracer can be determined through a location algorithm [190]. Firstly, the distances of a point perpendicular to all the gamma-ray trajectories are calculated. Secondly, the point that minimizes the sum of the distances is found. A typical measurement setup of PEPT on a fluidized bed is shown in Fig. 17 [191]. Two gamma-ray detectors of positron camera are placed on both sides of the bed, covering a field of 600×300 mm^2 and providing a spatial resolution of about 2 mm. The detectors are connected to a computer where the tracer positions are recorded in real-time. The tracer particles were made by resin beads selected from the bulk particles. An ion exchange technique was employed to active the tracers instead of bombarding them directly in a cyclotron. Based on the recorded tracer trajectories, particle velocity distribution was obtained by analysing separately the upward and downward movement data. The solids mixing behaviours, which were closely related to the motion of particles and bubbles, were also characterized from the particle velocity distribution maps.
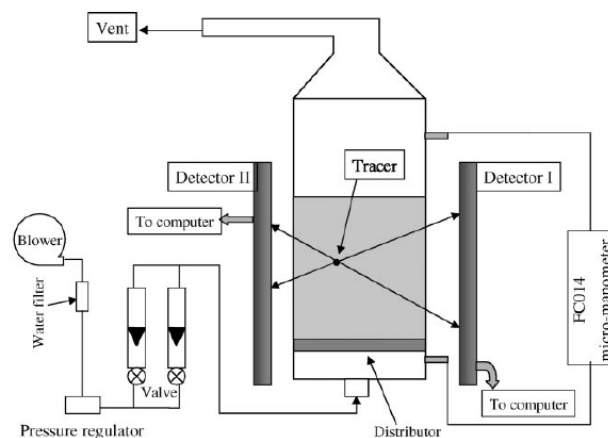

Fig. 17. PEPT system [191]

The identification of flow modes (or flow patterns) is of significance to the design and operation of fluidized bed reactors, where chemical conversions proceed with time. The mixed flow is required by most of the gas/solid reactions, while the plug flow is preferred by most catalytic gas phase reactions [192]. PEPT provides a straightforward approach to characterizing the flow modes and their transitions [192-194]. For example, when a mixed flow (or core-annulus flow) was formed in a riser, a dilute region with rapidly rising particles existed in the core of the riser, surrounded by a denser annulus of particles descending near the wall. The two different regions were clearly identified from the population density plots of the upward and downward moving particles on a cross-section [192]. When there was a plug flow, most of the particles moved upwards, and the downward flowing particles were randomly distributed on the cross-section [192]. PEPT also allowed the measurement of solids circulation flux in a CFB by following the tracer velocity within a given distance in the downcomer, with an assumption that the flow was in a moving packed-bed pattern [195]. Similarly, the dimensionless solids flux across the jet boundaries in a bubbling fluidized bed was determined from the tracer trajectory data [196]. In addition, based on the PEPT measured data distribution, a 'phase diagram' was proposed to depict different flow modes (e.g. dilute, dense, core-annulus and combined fluidization flows) as a function of the superficial gas velocity and solids circulation flux in a riser [197]. Other hydrodynamic properties in a fluidized bed such as the particle circulation frequency, particle RTD and flow structure

evolution can also be characterized using the PEPT measured data [191, 198-202]. Although bubble parameters cannot be directly determined through PEPT, it is feasible to deduce the bubble dynamic properties from the particle velocity data. Fan et al. [199, 203] obtained the bubble rising velocity and the associated sizes by this means, which demonstrated that PEPT was a potential way to characterize bubble behaviours.

PEPT supplies detailed information about particle flow in both the dense-and dilute-phase fluidized beds. The intrinsic capability of tracking particle motion also makes PEPT in principle suitable for the validation of DEM and DPM simulation [204, 205]. PEPT also possesses some advantages over RPT. Firstly, no calibration is required. Secondly, tracer positions are determined during the measurement rather than through reconstruction. Thirdly, the activity loss of the tracer does not need to be considered. Thirdly, the tracer particle is usually selected from the bulk of the fluidized materials, while the one utilized in RPT is specially made [202]. However, PEPT only allows the tracking of one single particle, giving rise to a long time to obtain the statistically reliable results representative for the bulk flow. Therefore, PEPT is unsuitable for real-time measurement. Another drawback of PEPT is that the apparatus is larger, less flexible and more expensive than that of RPT.

6. Laser Doppler anemometry and phase Doppler anemometry

A change of wave frequency caused by the relative motion between a wave source and a wave receiver is named the 'Doppler effect', based on which the laser

Doppler anemometry (LDA) and phase Doppler anemometry (PDA) have been developed to measure the particle velocity, size and concentration in multiphase flow systems. Since the LDA and PDA techniques have already been reviewed in detail in other work [102], we will give a brief introduction hereby. Fig. 18 shows a LDA/PDA measurement system, composed of a laser source, a beam splitter, transmitting and receiving optics, a light detector/detectors, a signal processor, an oscilloscope and a computer [206]. The output of the beam splitter is two beams of equal intensities but different frequencies. They are focused into optical fibers which bring them to a probe containing the transmitting optics. In this probe, the two parallel beams are focused through a lens into the measurement volume, where they intersect. The intersection generates a pattern of plane interference fringes [207]. If a particle passes through the intersection area, light will be scattered and its intensity will change due to the interference fringes. The scattered light is then collected by a receiving lens and focused on a detector or multiple detectors to produce a signal. Particle velocity is calculated from the Doppler frequency and the fringe distance. Besides, particle size is measured through PDA as an extension of LDA. Two adjacent detectors used to collect the scattered laser light show a phase difference, which is linearly proportional to the diameter of a smooth and spherical particle passing through the measurement volume. The particle diameter is then obtained from the phase shift, focal length, fringe spacing, optical constant and spacing between the detectors. Two approaches are available for the measurement of particle concentration. One is to use the data rate of the signal processor in the LDA system, which is suitable for dilute flow systems

[208]. The other is to use the time ratio between the time occupied by the dispersed phase and the total sampling time. This approach involves an assumption that only one particle is in the measurement volume at the same time, which makes it only applicable to very dilute systems. Readers can refer to the work of Mathiesen et al. [207] for more detailed information about the characterization of these particle-related hydrodynamic parameters.
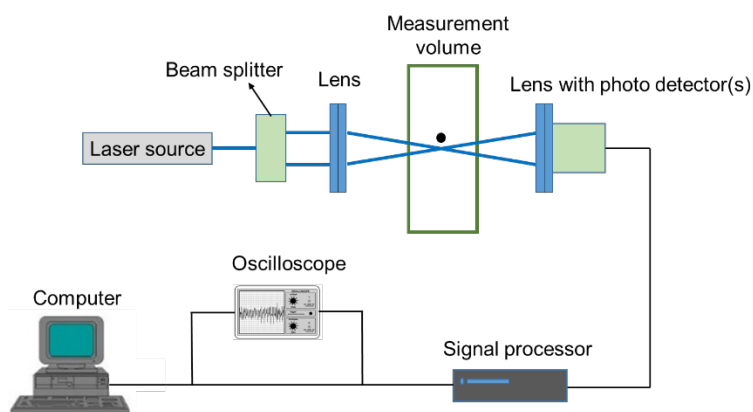
Fig. 18. LDA/PDA system [206]

Based on the aforementioned sensing principles, LDA and PDA are suitable for the measurement on dilute fluidization systems. There have been studies of the particle velocity distribution, particle size distribution as well as particle concentration profile in CFBs [209-212]. LDA and PDA were also utilized to assess the influence of the inlet and outlet configurations on the flow patterns and flow structures in a riser [213-215]. Besides, the particle shear stress and particle fluctuation energy were derived from the LDA measured velocity data [216].

LDA offers a potential solution to the measurement of a wide range of particle velocity from 0.1 mm/s to 100 m/s on an on-line continuous basis [14]. Its major

advantages are the high spatial resolution and fast dynamic response. PDA allows the measurement of particle size from the micron scale to millimetre scale with a good immunity to noise. However, this technique is only applicable under dilute flow conditions, and the maximum solids concentration depends on the laser power and the sensitivity of the signal processing equipment. If LDA and PDA are used for the dense flow measurement, light will be scattered outside the measurement volume by particles or even be blocked by the dense solids distribution. The data rate and signal-to-noise ratio will thus be significantly reduced. A possible way to eliminate this influence is to match the refraction index of some particles to that of the fluid, or to make the measurement intrusive at the expense of distorting the flow field [215]. An additional restriction of PDA is the requirement of smooth and spherical particles. In addition, LDA and PDA are unsuitable for the application in industrial beds because of their opaque walls. Even if an optical access is available, it is susceptible to contamination by particle adhesion.

7. Pressure fluctuation method

Pressure fluctuation is well-known as an important indicator for the hydrodynamic properties in a gas-solid fluidized bed. Due to the easy implementation and low cost, pressure fluctuation measurement has been widely employed to characterize fluidization behaviours. However, the interpretation of pressure signals is still far from straightforward due to the complexity of pressure fluctuation. Firstly, a local pressure fluctuation may originate from multiple sources, such as the fluctuation

from local bubbles, the global bed oscillation and the propagating pressure waves from other locations (e.g. bed surface, distributor and windbox), resulting in the intrinsically non-local nature of pressure fluctuation. Secondly, the complexity of local pressure signals is enhanced by the coupling relationships among the bubble motion, particle oscillation, bed surface oscillation, pressure wave propagation and flow pulsation [68]. Until now, the pressure fluctuation measurement has received widespread attentions and has been comprehensively reviewed. For example, Bi et al. [68] examined the pressure fluctuation phenomena in gas-solid fluidized beds and provided explanations of the underlying mechanisms. Sasic et al. [217] reviewed the modelling and experimental techniques for pressure signal acquisition. van Ommen and Mudde [218] elaborated different methods for the measurement of voidage distribution in fluidized beds, including the pressure fluctuation method. van Ommen et al. [219] reviewed the time-series analysis methods implemented on pressure fluctuation signals, as well as their applications to the monitoring and control of fluidized bed combustion and gasification [220]. In view of these specialized reviews, here we will briefly introduce the sensing principle and applications of the pressure fluctuation method to gas-solid fluidized beds.

A typical pressure fluctuation measurement setup is shown in Fig. 19. It is mainly composed of a pressure sensor (probe), a pressure transmitter, a data acquisition board and a computer. A fine mesh net is fixed on the probe tip, alternatively, a purge flow can be used to prevent particles from entering the probe. The pressure measurement can be considered as non-intrusive when the probe is placed flush to the inner wall of

the bed. Normally, the sampling frequency ranges from 10 Hz to 1000 Hz, and the sampling period is not less than 30 s [68].
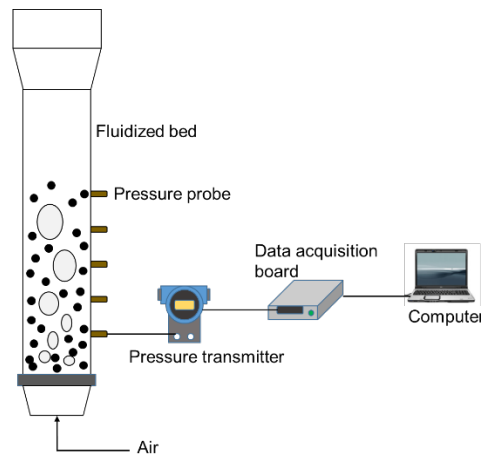
Fig. 19. Pressure fluctuation measurement system

In order to acquire the quantitative information about flow dynamics, the raw pressure signals are processed through different methods, such as time domain analysis, frequency domain analysis and state space analysis. van Ommen et al. [219] has discussed the applications of these methods extensively. The time domain analysis primarily includes the standard deviation and higher-order moments, probability distribution of pressure increments, cycle time, rescaled range analysis (or named the R/S or Hurst analysis) as well as the associated V-statistic and Autoregressive (AR) models. These methods were used to characterize the solids mass flux, flow regime transition, fluidization quality, particle size and variation, agglomerate occurrence as well as the degree of stochasticity in fluidized beds [221-224]. The most widely employed frequency domain analysis approach is the power spectrum, which can be obtained from the parametric or non-parametric method. In the parametric method, the

fluctuation data is firstly generated by a model and then processed by spectral estimation, while the non-parametric method makes no assumption on the data generation. The amplitude and dominant frequency of pressure signals are commonly used to characterize bubble size and frequency, respectively. The fall-off of the semi-logarithmic power spectrum is also an indicator of the dynamic behaviours in the fluidized bed. In addition, the wavelet transform and wavelet packets techniques are desirable tools for the multiscale analysis of pressure signals. They are used to extract the flow information about the time localization of particular frequency components. State space analysis is usually performed as a complementing method to the time and frequency domain analysis. For example, the attractor comparison method allows the detection of small changes in fluidization dynamics (e.g. agglomerate occurrence) with a higher sensitivity than other methods [219]. However, the commonly applied parameters in the state space analysis (e.g. entropy, correlation dimension and Lyapunov exponents) should be used prudently since their validity can be questionable if the conditions (e.g. independence of length scale) are not fulfilled.

Due to the complexity and multiscale nature of a fluidized bed, the pressure fluctuation signals collected typically contain multiscale hydrodynamic information. It is therefore important to resolve the pressure signals into multiple scales and identify the underlying contributing mechanisms. Extensive work has been conducted on this subject, using the signal processing methods ranging from simple statistical analysis to advanced chaotic and multiscale analysis, such as wavelet transform, Hurst analysis, time-delay embedding and Hilbert-Huang transform [68]. For instance, by

72

decomposing the pressure fluctuation signals into different scales, Zhao et al. [225] found that the microscale, mesoscale, and macroscale pressure fluctuation dynamics stemmed from the individual-particle motion and small-scale fluid eddies, the bubble-dense phase interactions, and the solids bulk motion at the bed scale, respectively. The pressure fluctuation mainly reflected the mesoscale interactions between the bubble and emulsion phases. However, Briongos et al. [226, 227] extracted different dynamic information from the pressure fluctuation signals through Hilbert-Huang transform. The first, third, and fifth empirical decomposition modes were found to correspond to the particle, bulk, and local-bubble scales, respectively. Therefore, more work is still required to achieve a consistent conclusion about the multiscale resolution of pressure signals.

The pressure fluctuation measurement is robust, cheap, virtually non-intrusive and easy for operation. It can withstand harsh industrial environments (e.g. high temperature, high pressure and dusty condition) and is therefore suitable for on-line monitoring and faults warning of industrial fluidized beds. However, limited by the intrinsically non-local and complex nature of the pressure fluctuation, the underlying mechanisms embedded in pressure signals are still lack of understanding. Especially for industrial fluidized beds, the pressure fluctuation depends on many operation conditions, such as gas superficial velocity fluctuation, particle size distribution, and condensate injection amount, making the pressure signal representation even more difficult. Besides, the low-amplitude compression pressure waves and bubble-passage pressure waves are only detectable within a limited area close to their origin. The

location and number of pressure sensors employed on an industrial fluidized bed should be optimized to collect valid data for further processing [228]. Until now, the typical pressure measurement applied on industrial fluidized beds is still the average pressure drop, and more work is required to achieve reliable multiscale representation of industrial pressure signals. Additionally, the information about particle motion can hardly be extracted from the pressure signals.

8. Trend and future developments

The non-intrusive measurement techniques as reviewed above have emerged as widespread and most attractive tools for the characterization of gas-solid fluidization behaviours. They provide useful, detailed information about a complex process without disturbing the flow field, which is crucial for understanding fluidization hydrodynamics, verifying CFD models as well as determining operational parameters. Table 1 summarizes the strengths and weaknesses of the non-intrusive techniques discussed in this review. Since no technique is capable of offering comprehensive flow information covering the hydrodynamic scales from the micro-level to macro-level, trade-off should be made in terms of the measurement scale of interest when determining suitable techniques. Other factors such as the ease of operation, ease of data interpretation, resolution, cost and applicability to industrial beds, should also be considered. Despite a variety of sensors and instruments based upon different principles proposed, few are currently working in industry. Apart from the intrinsic complexity of gas-solid fluidization systems, idealized assumptions and simplification

made by the researchers about the nature of flow field and plant operating conditions

are the major reasons for this underdevelopment.

Table 1 Comparison of the non-intrusive measurement techniques

Technique	Main measurable parameters	Ease of operati-on	Ease of data interpretation	Spatial resolution	Temporal resolution	Cost	Applicability in industrial beds
Electrostatic induction sensor	electrostatic charge, solids velocity, solids concentration	++	-	-	++	++	+
Faraday cup	electrostatic charges	+	++	/	/	+	--
AE sensor/ accelerometer	particle motion activity, particle size, bulk dynamics	++	-	o	++	++	++
Photography	bubble size, bubble holdup, bubble velocity, particle cluster size, cluster velocity	o	-	-	+	+	--
PIV	particle velocity, solids flux	-	o	+	+	-	--
X-ray radiography	bubble size, bubble holdup, bubble velocity	-	o	-	+	-	o
Gamma-ray densitometry	solids concentration, solids flux	-	+	o	+	-	o
ECT	solids concentration,	-	-	--	+	-	--

	bubble size, bubble velocity, bubble frequency						
X-ray CT	solids concentration	--	+	+	-	--	o
Ultrafast X-ray CT	solids concentration, bubble size, bubble velocity	--	+	+	+	--	o
Gamma-ray CT	solids concentration	--	+	+	-	--	o
NMRI	diffusivity, bed density, solids velocity, bubble size, bubble velocity, bubble frequency	--	o	+	+	--	--
IR thermography	temperature distribution, gas concentration	o	+	+	+	o	-
RPT	particle trajectory, solids flux	--	--	++	--	--	-
PEPT	particle trajectory, solid flux	--	--	++	--	--	-
LDA/PDA	particle velocity, particle size, solids concentration	--	o	++	+	--	--
Pressure fluctuation method	bubble or bulk dynamics, solids flux	++	o	--	++	++	++

Table 1 also shows that a wide range of techniques are available for the measurement of specific hydrodynamic parameters of gas and solids phases in a fluidized bed. For example, the bubble dynamic properties (e.g. size, rising velocity, coalescence/splitting) can be characterized through photography, X-ray radiography, ECT, ultrafast X-ray CT, NMRI, and pressure fluctuation method. Photography and X-ray radiography provide snapshots of bubble distribution in a fluidized bed. The original images captured always require post-processing, such as thresholding, indexing, and filtering false bubbles, to extract useful information about bubble dynamics. The temporal resolution of these two techniques is easily improved by employing high-speed image acquisition devices, however, the measurement accuracy depends on bubble superposition and wall-particle contamination, especially on a cylindrical fluidized bed. Pseudo and real 3D reconstructed images of bubble behaviors are provided by the traditional ECT and the ECVT techniques, respectively. It is worth mentioning that the vertical axis in a pseudo 3D reconstructed image represents the time instead of the length scale. In addition, the information about bubble frequency and velocity can be extracted from the solids concentration fluctuation signals collected from ECT. Similarly to ECT, ultrafast X-ray CT allows the characterization of bubble coalescence and breakup, bubble velocity, and pseudo 3D bubble shapes. NMRI provides bubble visualization merely in small-diameter (e.g. 50 mm) beds, and the particles under test must contain MR-sensitive nuclei (typically ^{1}H), which significantly limits the application of NMRI to bubble dynamics

characterization. The pressure fluctuation method is easy for operation and applicable to fluidized beds of various sizes. The bubble dynamic information (e.g. bubble size, bubble frequency) is acquired through pressure signal analysis. However, the interpretation of pressure signals is not straightforward due to the complexity of pressure fluctuation. Therefore, the measurement accuracy is strongly dependent on the signal processing methods employed. In addition, the spatial resolution of pressure fluctuation method is lower than the aforementioned techniques used for bubble characterization. As another example, the solids concentration can be characterized through electrostatic induction sensors, gamma-ray densitometry, ECT, X-ray CT, ultrafast X-ray CT, gamma-ray CT, LDA/PDA, and pressure fluctuation measurement, resulting in different information about solids distribution. Electrostatic sensors allow the characterization of relative solids concentration near the wall instead of the absolute value, whereas the pressure drop measured can be used to derive the axial profile of solids concentration. Gamma-ray densitometry results in line-averaged solids concentration at each chordal length or projection of the fluidized bed. ECT and X-ray/ ultrafast X-ray/ gamma-ray CT provide cross-sectional solids distribution information, despite their differences in the 'soft-field' and 'hard-field' measurement. LDA/PDA is only applicable to dilute flow conditions, and the maximum measurable solids concentration depends on the laser power and the sensitivity of signal processing equipment.

8.1. Sensors

At the current stage, a wide variety of sensors applied on gas-solid fluidized beds allow the measurement of solids/particle velocity, particle size, particle trajectory, solids concentration, bubble velocity, bubble dimension, cluster velocity, cluster size, electrostatic level, temperature distribution, diffusivity and some bulk dynamic properties. Each sensing principle mentioned in this review utilizes one of the physical properties of the solids or gas phase. Some are based on the intrinsic behaviours of the two-phase flow such as electrostatics, acoustic emission, vibration, thermal radiation and pressure fluctuation. Whereas others require stimulation or energy injection, such as X-ray, gamma-ray and nuclear magnetic resonance. Since no sensor can provide equally valid information covering the whole spectrum of flow scales, it is a promising solution to combine different sensors to enable data acquisition from the micro-level to macro-level. For example, electrostatic sensors, AE sensors and accelerometers are sensitive to particle motion; the low-frequency envelops of the signals from these sensors represent bulk dynamics in fluidized beds. Pressure sensors focus on the signals generated by bubble or bulk motion. Some visualization methods such as photography, ECT and X-ray/gamma-ray CT provide information about the whole sensing field. Apart from the combination of different sensors, the sensing elements set in a differential mode may be adaptable to new measurement techniques in future. Along with the continuous developments of the existing techniques, new sensor designs and applications are continuing to emerge. For instance, a Lagrangian sensor system, mainly composed of an accelerometer, a

magnetometer, a microcomputer and a wireless transmitter module, has recently been developed to measure the forces on a free-moving object in a bubbling fluidized bed [229]. The Lorentz force velocimetry, based on exposing the fluid under test to a magnetic field and measuring the drag force acting upon the magnetic field lines [230, 231], has now been applied to weakly conducting fluids for the measurement of velocity and flow rate [232, 233]. It is envisaged that the Lorentz force velocimetry will be used on gas-solid fluidized beds as a novel non-intrusive technique. An improvement of infrared thermography has also been proposed by employing propane as the tracer gas and quartz as the wall material, which allows the use of a relatively inexpensive configuration for the measurement of detailed concentration fields [234]. Moreover, integrated sensors operating on complementary sensing principles are to be developed that allow the measurement of different flow parameters simultaneously, without significant compromise on the measurement accuracy. However, this requires novel, or very likely more sophisticated, sensor design and manufacture as well as new signal processing techniques.

In an industrial fluidized bed, opaque walls and strong backmixing of particles usually invalidate the techniques that require optical access or dilute flow conditions, such as photography, PIV and LDA/PDA. Under hot and dusty conditions, particle accumulation in the sensing zone due to electrostatic adherence and particle agglomeration is also a serious practical problem. It is suggested that special means should be taken to keep the sensing surface clean, such as introducing the purge gas or installing a wiping mechanism into the sensor. Moreover, under a dense flow

condition, the ring-shape and arc-shape electrostatic induction sensors may no longer be applicable for the measurement of bulk solids velocity, since the signals from these sensors only reflect the particle motion characteristics near the wall. The chemical properties of solids also affect the measurement results from the sensors based on electrical, resonance and attenuation principles. For instance, variations in moisture content, environmental humidity and particle components introduce significant errors in the electrostatic measurement. Therefore, these sensors must be calibrated using the specific type of solids to be measured in the fluidized beds [235]. Amongst all the sensors mentioned, AE sensors, accelerometers and pressure sensors are suitable for the process monitoring and measurement under harsh industrial conditions. It is also promising to employ the ring- and arc-shaped electrostatic sensors in conjunction with the rod-shaped ones to probe the entire flow field on a cross-section of the fluidized bed. Since the techniques based on radiation, such as X-ray/gamma-ray CT, RPT and PEPT, can still work normally in an industrial environment, it is feasible to use them for on-line monitoring. Particularly, along with the advances in tomographic techniques, the fast and ultrafast X-ray CT can be utilized to capture the flow field snapshots in industrial fluidized beds. Cost-effective radiation-based instruments are also expected to emerge in future.

8.2. Signal and image processing

Signal processing is a crucial step to convert raw signals into useful information. There are numerous data analysis methods available for de-noising and extracting the

multiscale characteristic signals of a fluidization process. Signals in the form of time series are usually processed through time-domain analysis, frequency-domain analysis and state space analysis. Different analysis methods aim to resolve the signal series from different aspects. For instance, the standard deviation of AE signal represents the particle fluctuation intensity, while the wavelet transform on AE signal can be used to determine the particle size distribution. In view of the fast speed of signal processing, electrostatic sensors, AE sensors, accelerometers and pressure sensors are suitable and already used for the on-line monitoring and real-time measurement of industrial fluidized beds. Apart from the conventional signal processing approaches, some concepts and analysis methods originating from the turbulence theory are promising in characterizing the hydrodynamics of two-phase flow. Sun et al. [236, 237] employed the continuous wavelet transform, autocorrelation method and Extended Self Similarity (ESS) scaling law to analyze the particle fluctuation velocity signals, according to which the flow field intermittency and particle vortex evolution in a fluidized bed were characterized. Although this work was based on CFD simulation, the signal analysis methods can be applied directly to any fluctuating signal series from a sensor. On the other hand, signals in the form of pixels or those for image reconstruction require more complex processing procedures. For example, the thresholding and bubble tracking techniques are usually applied to the raw images obtained through photography or radiography to extract useful information, and reconstruction algorithms are required by tomographic techniques to produce cross-sectional distribution images. Computational modelling provides a useful tool to

help optimize the image processing algorithms, it is therefore suggested that the modelling results and prior knowledge of flow field should be combined with the processing algorithms to improve the measurement accuracy. In order to enable the on-line monitoring and real-time measurement of fluidization parameters through visualization, the speed of signal processing and image reconstruction has to be improved. Moreover, embedded image pre-processing and reconstruction architectures should be considered in future development.

9. Conclusions

Gas-solid fluidized beds are complex flow systems due to their nonlinear, multiphase and multiscale nature. In order to make reliable scale-up and operation optimization of a fluidized bed, it is of great significance to characterize the hydrodynamic properties accurately. However, it is challenging to depict a fluidization process unambiguously due to the diversities in possible phases, flow patterns and fluidization regimes. Dedicated techniques are therefore required for the measurement of both the global and local hydrodynamic parameters without disturbing the flow field. This review has attempted to present a wide selection of the non-intrusive measurement techniques applicable to gas-solid fluidized beds and define the state-of-the-art in the development of the techniques. The authors are aware that there are still inventions and publications not included in this paper for various reasons.

An ideal non-intrusive sensor should be reliable, robust, sensitive to flow changes, suitable for real-time measurement and low-cost. In view of these requirements,

sensors such as the AE sensor, accelerometer, electrostatic sensor and pressure sensor should be preferentially considered for applications to fluidized beds. Yet, more work is required to improve the signal-to-noise ratio and extract the characteristic information from the raw signals. Essentially, the signals related to various flow behaviours are hybrid and coupling, it is therefore logical to integrate different measurement techniques to obtain comprehensive flow information at different scales. When choosing suitable techniques for a given fluidized bed, we need to consider the required spatial and temporal resolutions, measurement constraints (e.g. dense or dilute flow condition, particle backmixing, temperature and pressure ranges), variables to be measured (e.g. time-averaged value or instantaneous reading) and expected accuracies. For an industrial bed, it is a potential way to combine the AE sensor/accelerometer, electrostatic sensor, pressure sensor and X-ray CT together to characterize the averaged and instantaneous variables both locally and globally. Furthermore, with the continuous advances in new materials, electronic components and computing techniques, it is feasible to develop a sensor in which multiple measurement functions are integrated. Correspondingly, different data processing techniques should be applied in parallel to analyze the signals stemmed from different flow behaviours. It will be interesting to see the further developments and applications of non-intrusive measurement techniques to the characterization of fluidization systems in the next decade.

Acknowledgements

References

1.	Busciglio A, Vella G, Micale G, Rizzuti L. Analysis of the bubbling behaviour of 2D gas solid fluidized beds Part II. Comparison between experiments and numerical simulations via Digital Image Analysis Technique. Chem Eng J. 2009;148(1):145-63.

2.	Liu S, Chen Q, Wang HG, Jiang F, Ismail I, Yang WQ. Electrical capacitance tomography for gas-solids flow measurement for circulating fluidized beds. Flow Meas Instrum. 2005;16(2-3):135-44.

3.	Wu BY, Kantzas A, Bellehumeur CT, He ZX, Kryuchkov S. Multiresolution analysis of pressure fluctuations in a gas-solids fluidized bed: Application to glass beads and polyethylene powder systems. Chem Eng J. 2007;131(1-3):23-33.

4.	Letzel HM, Schouten JC, Krishna R, van den Bleek CM. Characterization of regimes and regime transitions in bubble columns by chaos analysis of pressure signals. Chem Eng Sci. 1997;52(24):4447-59.

5.	Bi HTT, Li JH. Multiscale analysis and modeling of multiphase chemical reactors. Adv Powder Technol. 2004;15(6):607-27.

6.	Karimi M, Mostoufi N, Zarghami R, Sotudeh-Gharebagh R. Nonlinear dynamics of a gas-solid fluidized bed by the state space analysis. Chem Eng Sci. 2011;66(20):4645-53.

7.	He YJ, Wang JD, Cao YJ, Yang YR. Resolution of Structure Characteristics of AE Signals in Multiphase Flow System-From Data to Information. Aiche J. 2009;55(10):2563-77.

8.	Geldart D. Types of Gas Fluidization. Powder Technol. 1973;7(5):285-92.

9.	Tanfara H, Pugsley T, Winters C. Effect of particle size distribution on local voidage in a bench-scale conical fluidized bed dryer. Dry Technol. 2002;20(6):1273-89.

10.	Lin CL, Wey MY. Statistical and power spectral analysis of quality of fluidization for different particle size distributions at high temperature. Adv Powder Technol. 2004;15(1):79-96.

11.	Deen NG, Peters EAJF, Padding JT, Kuipers JAM. Review of direct numerical simulation of fluid-particle mass, momentum and heat transfer in dense gas-solid flows. Chem Eng Sci. 2014;116:710-24.

12.	Jin Y, Zhu, J.X., Wang, Z.W., Yu, Z.Q. Fluidization Engineering Principles. Beijing: Tsinghua University Press; 2001.

13.	Cen KF. Theoretical design and operation of circulating fluidized bed boilers. Beijing: China Electric Power Press; 1998.

14.	Yan Y. Mass flow measurement of bulk solids in pneumatic pipelines. Meas Sci Technol.

1996;7(12):1687-706.

15. Werther J. Measurement techniques in fluidized beds. Powder Technol. 1999;102(1):15-36.

16. Tayebi D, Svendsen HF, Jakobsen HA, Grislingas A. Measurement techniques and data interpretations for validating CFD multi phase reactor models. Chem Eng Commun. 2001;186:57-159.

17. Sowinski A, Salama F, Mehrani P. New technique for electrostatic charge measurement in gas-solid fluidized beds. J Electrostat. 2009;67(4):568-73.

18. Hendrickson G. Electrostatics and gas phase fluidized bed polymerization reactor wall sheeting. Chem Eng Sci. 2006;61(4):1041-64.

19. Wang F, Wang JD, Yang YR. Distribution of Electrostatic Potential in a Gas-Solid Fluidized Bed and Measurement of Bed Level. Ind Eng Chem Res. 2008;47(23):9517-26.

20. Mehrani P, Bi HT, Grace JR. Electrostatic behavior of different fines added to a Faraday cup fluidized bed. J Electrostat. 2007;65(1):1-10.

21. Wang JD, Xu Y, Li W, Yang YR, Wang F. Electrostatic potentials in gas-solid fluidized beds influenced by the injection of charge inducing agents. J Electrostat. 2009;67(5):815-26.

22. Moughrabiah WO, Grace JR, Bi XT. Effects of Pressure, Temperature, and Gas Velocity on Electrostatics in Gas-Solid Fluidized Beds. Ind Eng Chem Res. 2009;48(1):320-5.

23. Sowinski A, Miller L, Mehrani P. Investigation of electrostatic charge distribution in gas-solid fluidized beds. Chem Eng Sci. 2010;65(9):2771-81.

24. Salama F, Sowinski A, Atieh K, Mehrani P. Investigation of electrostatic charge distribution within the reactor wall fouling and bulk regions of a gas-solid fluidized bed. J Electrostat. 2013;71(1):21-7.

25. Dong KZ, Zhang Q, Huang ZL, Liao ZW, Wang JD, Yang YR. Experimental Investigation of Electrostatic Reduction in a Gas-Solid Fluidized Bed by an in Situ Corona Charge Eliminator. Ind Eng Chem Res. 2014;53(37):14217-24.

26. Dong KZ, Zhang, Q., Huang, Z. L., Liao, Z. W., Wang, J. D., Yang, Y. R., Wang, F. Experimental investigation of electrostatic effect on particle motions in gas-solid fluidized beds. AIChE Journal. 2015;61(11):3628-38.

27. Ma J, Yan Y. Design and evaluation of electrostatic sensors for the measurement of velocity of pneumatically conveyed solids. Flow Measurement and Instrumentation. 2000;11(3):195-204.

28. Yan Y, Xu LJ, Lee P. Mass flow measurement of fine particles in a pneumatic suspension using electrostatic sensing and neural network techniques. Ieee T Instrum Meas. 2006;55(6):2330-4.

29. Qian XC, Yan Y, Shao JQ, Wang LJ, Zhou H, Wang C. Quantitative characterization of pulverized coal and biomass-coal blends in pneumatic conveying pipelines using electrostatic sensor arrays and data fusion techniques. Meas Sci Technol. 2012;23(8).

30. Qian XC, Huang XB, Hu YH, Yan Y. Pulverized coal flow metering on a full-scale power plant using electrostatic sensor arrays. Flow Meas Instrum. 2014;40:185-91.

31. Gajewski JB. Non-contact electrostatic flow probes for measuring the flow rate and charge in the two-phase gas-solids flows. Chem Eng Sci. 2006;61(7):2262-70.

32. Xu CL, Liang C, Zhou B, Wang SM. HHT analysis of electrostatic fluctuation signals in dense-phase pneumatic conveying of pulverized coal at high pressure. Chem Eng Sci. 2010;65(4):1334-44.

33. Yan Y, Byrne B, Woodhead S, Coulthard J. Velocity-Measurement of Pneumatically

Conveyed Solids Using Electrodynamic Sensors. Meas Sci Technol. 1995;6(5):515-37.

34.   Zhang WB, Cheng YP, Wang C, Yang WQ, Wang CH. Investigation on Hydrodynamics of Triple-Bed Combined Circulating Fluidized Bed Using Electrostatic Sensor and Electrical Capacitance Tomography. Ind Eng Chem Res. 2013;52(32):11198-207.

35.   Zhang WB, Yan, Y., Yang, Y. R., Wang, J. D. Measurement of flow parameters in a bubbling fluidized bed using electrostatic sensor arrays International Instrumentation and Measurement Technology Conference; Pisa, Italy2015.

36.   Park AH, Bi HS, Grace JR. Reduction of electrostatic charges in gas-solid fluidized beds. Chem Eng Sci. 2002;57(1):153-62.

37.   Liu ZL, Bi XTT, Grace JR. Electrostatic charging behaviour of dielectric particles in a pressurized gas-solid fluidized bed. J Electrostat. 2010;68(4):321-7.

38.   Moughrabiah WO, Grace JR, Bi XT. Electrostatics in gas-solid fluidized beds for different particle properties. Chem Eng Sci. 2012;75:198-208.

39.   He C, Bi XTT, Grace JR. Simultaneous measurements of particle charge density and bubble properties in gas-solid fluidized beds by dual-tip electrostatic probes. Chem Eng Sci. 2015;123:11-21.

40.   Chen AH, Bi HT, Grace JR, van Willigen FK, van Ommen JR. Measurement of charge distribution around a rising bubble in a 2-D fluidized bed. Aiche J. 2006;52(1):174-84.

41.   Chen A, Bi HT, Grace JR. Charge distribution around a rising bubble in a two-dimensional fluidized bed by signal reconstruction. Powder Technology. 2007;177(3):113-24.

42.   Coombes J, Yan Y. Experimental investigations into the flow characteristics of pneumatically conveyed biomass particles using an electrostatic sensor array. Fuel. 2015;151:11-20.

43.   Zhao H, Castle GSP, Inculet II, Bailey AG. Bipolar charging in polydisperse polymer powders in industrial processes. Ieee Ind Applic Soc. 2000:835-41.

44.   Mehrani P, Bi HT, Grace JR. Electrostatic charge generation in gas-solid fluidized beds. J Electrostat. 2005;63(2):165-73.

45.   Gao L, Yan Y, Sun D, Qian X, Xu C, editors. In-line continuous sizing of biomass particles in gas-solid two-phase flow at a biomass-fired power plant. 8th International Symposium on Measurement Techniques for Multiphase Flows; 2013; Guangzhou, P.R. China.

46.   Boyd JWR, Varley J. The uses of passive measurement of acoustic emissions from chemical engineering processes. Chem Eng Sci. 2001;56(5):1749-67.

47.   McClements DJ. Ultrasonic characterization of foods and drinks: Principles, methods, and applications. Critical Reviews in Food Science and Nutrition. 1997;37(1):1-46.

48.   Briongos JV, Aragon JM, Palancar MC. Fluidised bed dynamics diagnosis from measurements of low-frequency out-bed passive acoustic emissions. Powder Technol. 2006;162(2):145-56.

49.   Zukowski W. A simple model for explosive combustion of premixed natural gas with air in a bubbling fluidized bed of inert sand. Combust Flame. 2003;134(4):399-409.

50.   Zukowski W. An acoustic method of studying sequential explosions during gas combustion in bubbling fluidized beds. Combustion and Flame. 2001;125(3):1075-82.

51.   Salehi-Nik N, Sotudeh-Gharebagh R, Mostoufi N, Zarghami R, Mahjoob MJ. Determination of hydrodynamic behavior of gas-solid fluidized beds using statistical analysis of acoustic emissions. Int J Multiphas Flow. 2009;35(11):1011-6.

52.   Book G, Albion K, Briens L, Briens C, Berruti F. On-line detection of bed fluidity in

gas-solid fluidized beds with liquid injection by passive acoustic and vibrometric methods. Powder Technol. 2011;205(1-3):126-36.

53. Jiang XJ, Wang JD, Jiang BB, Yang YR, Hou LX. Study of the power spectrum of acoustic emission (AE) by accelerometers in fluidized beds. Ind Eng Chem Res. 2007;46(21):6904-9.

54. Ren CJ, Wang JD, Song D, Jiang BB, Liao ZW, Yang YR. Determination of particle size distribution by multi-scale analysis of acoustic emission signals in gas-solid fluidized bed. J Zhejiang Univ-Sc A. 2011;12(4):260-7.

55. Wang JD, Ren CJ, Yang YR, Hou LX. Characterization of Particle Fluidization Pattern in a Gas Solid Fluidized Bed Based on Acoustic Emission (AE) Measurement. Ind Eng Chem Res. 2009;48(18):8508-14.

56. Wang JD, Ren CJ, Yang YR. Characterization of Flow Regime Transition and Particle Motion Using Acoustic Emission Measurement in a Gas-Solid Fluidized Bed. Aiche J. 2010;56(5):1173-83.

57. Li YQ, Grace JR, Gopaluni RB, Bi HT, Lim CJ, Ellis N. Characterization of gas-solid fluidization: A comparative study of acoustic and pressure signals. Powder Technol. 2011;214(2):200-10.

58. de Martin L, Briongos JV, Aragon JM, Palancar MC. Can low frequency accelerometry replace pressure measurements for monitoring gas-solid fluidized beds? Chem Eng Sci. 2010;65(13):4055-64.

59. Gidaspow D, Huilin L. Equation of state and radial distribution functions of FCC particles in a CFB. Aiche J. 1998;44(2):279-93.

60. Cody WK. On the requirements for a metaparadigm: An invitation to dialogue - Response. Nurs Sci Quart. 1996;9(3):97-9.

61. Cody GD, Bellows RJ, Goldfarb DJ, Wolf HA, Storch GV. A novel non-intrusive probe of particle motion and gas generation in the feed injection zone of the feed riser of a fluidized bed catalytic cracking unit. Powder Technol. 2000;110(1-2):128-42.

62. Zhou YF, Ren CJ, Wang JD, Yang YR. Characterization on Hydrodynamic Behavior in Liquid-Containing Gas-Solid Fluidized Bed Reactor. Aiche J. 2013;59(4):1056-65.

63. de Martin L, Briongos JV, Garcia-Hernando N, Aragon JM. Detecting regime transitions in gas-solid fluidized beds from low frequency accelerometry signals. Powder Technol. 2011;207(1-3):104-12.

64. Bartels M, Lin WG, Nijenhuis J, Kapteijn F, van Ommen JR. Agglomeration in fluidized beds at high temperatures: Mechanisms, detection and prevention. Prog Energ Combust. 2008;34(5):633-66.

65. Briongos JV, Sobrino C, Gomez-Hernandez J, Santana D. Characterization of flow-induced vibrations in gas-solid fluidized beds: Elements of the theory. Chem Eng Sci. 2013;93:181-96.

66. Abbasi M, Sotudeh-Gharebagh R, Mostoufi N, Mahjoob MJ. Non-intrusive monitoring of bubbles in a gas-solid fluidized bed using vibration signature analysis. Powder Technol. 2009;196(3):278-85.

67. Azizpour H, Sotudeh-Gharebagh R, Zarghami R, Abbasi M, Mostoufi N, Mahjoob MJ. Characterization of gas-solid fluidized bed hydrodynamics by vibration signature analysis. Int J Multiphas Flow. 2011;37(7):788-93.

68. Bi HTT. A critical review of the complex pressure fluctuation phenomenon in gas-solids fluidized beds. Chem Eng Sci. 2007;62(13):3473-93.

69. Gera DG, M. Bubble rise velocity in two dimensional fluidized beds. Powder Technol.

1995;84(3):283-5.

70.   Caicedo GR, Marques JJP, Ruiz MG, Soler JG. A study on the behaviour of bubbles of a 2D gas-solid fluidized bed using digital image analysis. Chemical Engineering and Processing. 2003;42(1):9-14.

71.   Busciglio A, Vella G, Micale G, Rizzuti L. Analysis of the bubbling behaviour of 2D gas solid fluidized beds Part I. Digital image analysis technique. Chem Eng J. 2008;140(1-3):398-413.

72.   Zhu C, Yu Q, Dave RN, Pfeffer R. Gas fluidization characteristics of nanoparticle agglomerates. Aiche J. 2005;51(2):426-39.

73.   Wang XS, Palero V, Soria J, Rhodes MJ. Laser-based planar imaging of nano-particle fluidization: Part I - determination of aggregate size and shape. Chem Eng Sci. 2006;61(16):5476-86.

74.   Soler JG, Marques JJP, Ruiz MG, Caicedo GR. Calibration of the method to measure bubble properties in 2D fluidized beds. Chem Eng Commun. 2003;190(3):285-98.

75.   Movahedirad S, Dehkordi AM, Molaei EA, Haghi M, Banaei M, Kuipers JAM. Bubble Splitting in a Pseudo-2D Gas-Solid Fluidized Bed for Geldart B-Type Particles. Chemical Engineering & Technology. 2014;37(12):2096-102.

76.   Cabezas-Gomez L, da Silva RC, Navarro HA, Milioli FE. Cluster identification and characterization in the riser of a circulating fluidized bed from numerical simulation results. Applied Mathematical Modelling. 2008;32(3):327-40.

77.   Horio M, Kuroki, H. Three-dimensional flow visualization of dilutely dispersed solids in bubbling and circulating fluidized beds. Chem Eng Sci. 1994;49(15):2413-21.

78.   Berguerand N, Lyngfelt A. Design and operation of a 10 kW(th) chemical-looping combustor for solid fuels - Testing with South African coal. Fuel. 2008;87(12):2713-26.

79.   Quintanilla MAS, Valverde JM, Espin MJ, Castellanos A. Electrofluidization of Silica Nanoparticle Agglomerates. Ind Eng Chem Res. 2012;51(1):531-8.

80.   Wang S, Liu, G., Zhao, F., Zhang, Q., Lu, H. Modeling of clusters characteristics in circulating fluidized beds. CIESC J. 2014;65(6):2027-33.

81.   Chew JW, Parker DM, Cocco RA, Hrenya CM. Cluster characteristics of continuous size distributions and binary mixtures of Group B particles in dilute riser flow. Chem Eng J. 2011;178:348-58.

82.   Davidson JF. Circulating fluidised bed hydrodynamics. Powder Technol. 2000;113(3):249-60.

83.   Lackermeier U, Rudnick C, Werther J, Bredebusch A, Burkhardt H. Visualization of flow structures inside a circulating fluidized bed by means of laser sheet and image processing. Powder Technol. 2001;114(1-3):71-83.

84.   Gidaspow D, Lu HL. Collisional viscosity of FCC particles in a CFB. Aiche J. 1996;42(9):2503-10.

85.   Tartan M, Gidaspow D. Measurement of granular temperature and stresses in risers. Aiche J. 2004;50(8):1760-75.

86.   Laverman JA, Roghair I, Annaland MV, Kuipers H. Investigation into the hydrodynamics of gas-solid fluidized beds using particle image velocimetry coupled with digital image analysis. Can J Chem Eng. 2008;86(3):523-35.

87.   Kashyap M, Gidaspow D. Computation and measurements of mass transfer and dispersion coefficients in fluidized beds. Powder Technol. 2010;203(1):40-+.

88.   Kashyap M, Gidaspow D. Circulation of Geldart D type particles: Part II-Low solids fluxes

Measurements and computation under dilute conditions. Chem Eng Sci. 2011;66(8):1649-70.

89. Sutkar VS, Deen NG, Salikov V, Antonyuk S, Heinrich S, Kuipers JAM. Experimental and numerical investigations of a pseudo-2D spout fluidized bed with draft plates. Powder Technol. 2015;270:537-47.

90. van Buijtenen MS, Borner M, Deen NG, Heinrich S, Antonyuk S, Kuipers JAM. An experimental study of the effect of collision properties on spout fluidized bed dynamics. Powder Technol. 2011;206(1-2):139-48.

91. de Jong JF, Odu SO, van Buijtenen MS, Deen NG, Annaland MV, Kuipers JAM. Development and validation of a novel Digital Image Analysis method for fluidized bed Particle Image Velocimetry. Powder Technol. 2012;230:193-202.

92. Gidaspow D, Jung JW, Singh RK. Hydrodynamics of fluidization using kinetic theory: an emerging paradigm 2002 Flour-Daniel lecture. Powder Technol. 2004;148(2-3):123-41.

93. Jung J, Gidaspow D, Gamwo IK. Measurement of two kinds of granular temperatures, stresses, and dispersion in bubbling beds. Ind Eng Chem Res. 2005;44(5):1329-41.

94. Measurements and computation of dispersion and mass transfer coefficients in fluidized beds, (2010).

95. Breault RW. A review of gas-solid dispersion and mass transfer coefficient correlations in circulating fluidized beds. Powder Technol. 2006;163(1-2):9-17.

96. Kashyap M, Gidaspow D. Measurements of Dispersion Coefficients for FCC Particles in a Free Board. Ind Eng Chem Res. 2011;50(12):7549-65.

97. Heindel TJ. A Review of X-Ray Flow Visualization With Applications to Multiphase Flows. J Fluid Eng-T Asme. 2011;133(7).

98. Grassler T, Wirth KE. X-ray computer tomography - potential and limitation for the measurement of local solids distribution in circulating fluidized beds. Chem Eng J. 2000;77(1-2):65-72.

99. Hulme I, Kantzas A. Determination of bubble diameter and axial velocity for a polyethylene fluidized bed using X-ray fluoroscopy. Powder Technol. 2004;147(1-3):20-33.

100. Huilin L, Gidaspow D, Bouillard JX. Dimension measurements of hydrodynamic attractors in circulating fluidized beds. Powder Technol. 1997;90(3):179-85.

101. Cartz L. Nondestructive Testing. ASM International, Materials Park, OH.; 1995.

102. Chaouki J, Larachi F, Dudukovic MP. Noninvasive tomographic and velocimetric monitoring of multiphase flows. Ind Eng Chem Res. 1997;36(11):4476-503.

103. Yates JG, Cheesman DJ, Sergeev YA. Experimental-Observations of Voidage Distribution around Bubbles in a Fluidized-Bed. Chem Eng Sci. 1994;49(12):1885-95.

104. Schlieper D. Principles of gamma ray densitometry. Metal Powder Report. 2000;55(12):20-3.

105. Bhusarapu S, Fongarland P, Al-Dahhan MH, Dudukovic MP. Measurement of overall solids mass flux in a gas-solid circulating fluidized bed. Powder Technol. 2004;148(2-3):158-71.

106. Jiradilok V, Gidaspow D, Kalra J, Damronglerd S, Nitivattananon S. Explosive dissemination and flow of nanoparticles. Powder Technol. 2006;164(1):33-49.

107. Kashyap M, Gidaspow D, Koves WJ. Circulation of Geldart D type particles: Part I - High solids fluxes. Measurements and computation under solids slugging conditions. Chem Eng Sci. 2011;66(2):183-206.

108. Gidaspow D, Driscoll M. Porosity and Pressure Waves in a Fluidized Bed of FCC Particles.

Ind Eng Chem Res. 2009;48(5):2422-9.

109. Babelli IMM. Development of the multiphase meter using gamma densitometer concept. Proc Int Nucl Conf; Kuala Lumpur1997. p. 371-89.

110. Sutton MD. Tomographic techniques for the study of exceptionally preserved fossils. P Roy Soc B-Biol Sci. 2008;275(1643):1587-93.

111. Chaouki J, Larachi, F., Dudukovic, M. P. Computer assisted gamma and X-ray tomography: applications to multiphase flow systems. Non-Invasive Monitoring of Multiphase Flows: Elsevier Science; 1997.

112. Porzuczek J. Applications of Electrical Capacitance Tomography for Research on Phenomena Occurring in the Fluidised Bed Reactors. Chem Process Eng-Inz. 2014;35(4):397-408.

113. Yang WQ, Peng LH. Image reconstruction algorithms for electrical capacitance tomography. Meas Sci Technol. 2003;14(1):R1-R13.

114. Chandrasekera TC, Li Y, Moody D, Schnellmann MA, Dennis JS, Holland DJ. Measurement of bubble sizes in fluidised beds using electrical capacitance tomography. Chem Eng Sci. 2015;126:679-87.

115. Weber JM, Mei JS. Bubbling fluidized bed characterization using Electrical Capacitance Volume Tomography (ECVT). Powder Technol. 2013;242:40-50.

116. Warsito W, Fan L-S., editor Development of three-dimensional electrical capacitance tomography based on neural network multi-criterion optimization image reconstruction 3rd World Congress on Industrial Process Tomography; 2003; Banff, Canada.

117. Warsito W, Marashdeh, W., Fan, L-S., editor Electrical capacitance volume tomography (ECVT): sensor design and image reconstruction. 4th World Congress on Industrial Process Tomography; 2005; Aizu, Japan.

118. Warsito W, Marashdeh Q, Fan LS. Electrical capacitance volume tomography. Ieee Sens J. 2007;7(3-4):525-35.

119. Marashdeh Q, Fan LS, Du B, Warsito W. Electrical capacitance tomography - A perspective. Industrial & Engineering Chemistry Research. 2008;47(10):3708-19.

120. Peng LH, Ye JM, Lu G, Yang WQ. Evaluation of Effect of Number of Electrodes in ECT Sensors on Image Quality. Ieee Sens J. 2012;12(5):1554-65.

121. Du B, Fan LS, Wei F, Warsito W. Gas and solids mixing in a turbulent fluidized bed. Aiche J. 2002;48(9):1896-909.

122. Du B, Warsito W, Fan LS. ECT studies of gas-solid fluidized beds of different diameters. Ind Eng Chem Res. 2005;44(14):5020-30.

123. Du B, Warsito W, Fan LS. Bed nonhomogeneity in turbulent gas-solid fluidization. Aiche J. 2003;49(5):1109-26.

124. Du B, Warsito W, Fan LS. ECT studies of the choking phenomenon in a gas-solid circulating fluidized bed. Aiche J. 2004;50(7):1386-406.

125. Bing D, Fan LS. Characteristics of choking behavior in circulating fluidized beds for group B particles. Ind Eng Chem Res. 2004;43(18):5507-20.

126. Du B, Warsito W, Fan LS. Imaging the choking transition in gas-solid risers using electrical capacitance tomography. Ind Eng Chem Res. 2006;45(15):5384-95.

127. Du B, Warsito W, Fan LS. Behavior of the dense-phase transportation regime in a circulating fluidized bed. Ind Eng Chem Res. 2006;45(10):3741-51.

128. Wang F, Yu Z, Marashdeh Q, Fan LS. Horizontal gas and gas/solid jet penetration in a gas-solid fluidized bed. Chem Eng Sci. 2010;65(11):3394-408.

129. Qiu GZ, Ye JM, Wang HG, Yang WQ. Investigation of flow hydrodynamics and regime transition in a gas-solids fluidized bed with different riser diameters. Chem Eng Sci. 2014;116:195-207.

130. Makkawi Y, Wright P. Electrical capacitance tomography for conventional fluidized bed measurements—remarks on the measuring technique. Powder Technol. 2004;148(2-3):142-57.

131. Cai RR, Zhang YG, Li QH, Meng AH. Experimental characterizing the residence time distribution of large spherical objects immersed in a fluidized bed. Powder Technol. 2014;254:22-9.

132. Malcus S, Chaplin G, Pugsley T. The hydrodynamics of the high-density bottom zone in a CFB riser analyzed by means of electrical capacitance tomography (ECT). Chem Eng Sci. 2000;55(19):4129-38.

133. Makkawi YT, Wright PC. Fluidization regimes in a conventional fluidized bed characterized by means of electrical capacitance tomography. Chem Eng Sci. 2002;57(13):2411-37.

134. Rautenbach C, Melaaen MC, Halvorsen BM. Statistical diagnosis of a gas-solid fluidized bed using Electrical Capacitance Tomography. Int J Multiphas Flow. 2013;49:70-7.

135. Zhang WB, Wang C, Yang WQ, Wang CH. Application of electrical capacitance tomography in particulate process measurement - A review. Adv Powder Technol. 2014;25(1):174-88.

136. Wang HG, Yang WQ, Dyakowski T, Liu S. Study of bubbling and slugging fluidized beds by simulation and ECT. Aiche J. 2006;52(9):3078-87.

137. Lehner P, Wirth KE. Characterization of the flow pattern in a downer reactor. Chem Eng Sci. 1999;54(22):5471-83.

138. Bieberle M, Barthel F, Hampel U. Ultrafast X-ray computed tomography for the analysis of gas-solid fluidized beds. Chem Eng J. 2012;189:356-63.

139. Verma V, Padding JT, Deen NG, Kuipers JAM, Barthel F, Bieberle M, et al. Bubble dynamics in a 3-D gas-solid fluidized bed using ultrafast electron beam X-ray tomography and two-fluid model. Aiche J. 2014;60(5):1632-44.

140. Saayman J, Nicol W, Van Ommen JR, Mudde RF. Fast X-ray tomography for the quantification of the bubbling-, turbulent-and fast fluidization-flow regimes and void structures. Chem Eng J. 2013;234:437-47.

141. Toye D, Marchot P, Crine M, LHomme G. Modelling of multiphase flow in packed beds by computer-assisted x-ray tomography. Meas Sci Technol. 1996;7(3):436-43.

142. Patel AK, Waje SS, Thorat BN, Mujumdar AS. Tomographic diagnosis of gas maldistribution in gas-solid fluidized beds. Powder Technol. 2008;185(3):239-50.

143. Dudukovic MP. Opaque multiphase reactors: Experimentation, modeling and troubleshooting. Oil Gas Sci Technol. 2000;55(2):135-58.

144. Maccuaig N, Seville JPK, Gilboy WB, Clift R. Application of Gamma-Ray Tomography to Gas-Fluidized Beds. Appl Optics. 1985;24(23):4083-5.

145. VanLandeghem F, Nevicato D, Pitault I, Forissier M, Turlier P, Derouin C, et al. Fluid catalytic cracking: Modelling of an industrial riser. Appl Catal a-Gen. 1996;138(2):381-405.

146. Bhusarapu S, Al-Dahhan MH, Dudukovic MP. Solids flow mapping in a gas-solid riser: Mean holdup and velocity fields. Powder Technol. 2006;163(1-2):98-123.

147. Mudde RF. Advanced Measurement Techniques for Gls Reactors. Can J Chem Eng.

2010;88(4):638-47.

148. Holland DJ, Muller CR, Dennis JS, Gladden LF, Sedennan AJ. Spatially resolved measurement of anisotropic granular temperature in gas-fluidized beds. Powder Technol. 2008;182(2):171-81.

149. Pore M, Chandrasekera TC, Holland DJ, Wang AN, Wang F, Marashdeh Q, et al. Magnetic resonance studies of jets in a gas-solid fluidised bed. Particuology. 2012;10(2):161-9.

150. Savelsberg R, Demco DE, Blumich B, Stapf S. Particle motion in gas-fluidized granular systems by pulsed-field gradient nuclear magnetic resonance. Phys Rev E. 2002;65(2).

151. Fennell PS, Davidson JF, Dennis JS, Gladden LF, Hayhurst AN, Mantle MD, et al. A study of the mixing of solids in gas-fluidized beds, using ultra-fast MRI. Chem Eng Sci. 2005;60(7):2085-8.

152. Muller CR, Davidson JF, Dennis JS, Fennell PS, Gladden LF, Hayhurst AN, et al. Real-time measurement of bubbling phenomena in a three-dimensional gas-fluidized bed using ultrafast magnetic resonance imaging. Physical Review Letters. 2006;96(15).

153. Muller CR, Holland DJ, Davidson JF, Dennis JS, Gladden LF, Hayhurst AN, et al. Rapid two-dimensional imaging of bubbles and slugs in a three-dimensional, gas-solid, two-phase flow system using ultrafast magnetic resonance. Phys Rev E. 2007;75(2).

154. Muller CR, Holland DJ, Sederman AJ, Scott SA, Dennis JS, Gladden LF. Granular temperature: Comparison of Magnetic Resonance measurements with Discrete Element Model simulations. Powder Technol. 2008;184(2):241-53.

155. Muller CR, Holland DJ, Davidson JF, Dennis JS, Gladden LF, Hayhurst AN, et al. Geometrical and Hydrodynamical Study of Gas Jets in Packed and Fluidized Beds Using Magnetic Resonance. Can J Chem Eng. 2009;87(4):517-25.

156. Pore M, Holland DJ, Chandrasekera TC, Muller CR, Sederman AJ, Dennis JS, et al. Magnetic resonance studies of a gas-solids fluidised bed: Jet-jet and jet-wall interactions. Particuology. 2010;8(6):617-22.

157. Pavlin T, Wang R, McGorty R, Rosen MS, Cory DG, Candela D, et al. Noninvasive measurements of gas exchange in a three-dimensional fluidized bed by hyperpolarized Xe-129 NMR. Applied Magnetic Resonance. 2007;32(1-2):93-112.

158. Wang RP, Rosen MS, Candela D, Mair RW, Walsworth RL. Study of gas-fluidization dynamics with laser-polarized Xe-129. Magn Reson Imaging. 2005;23(2):203-7.

159. Pore M, Materazzi M, Chandrasekera TC, Holland DJ, Lettieri P, Sederman AJ, et al., editors. Using complimentary imaging techniques: X-ray and MRI studies of a bubbling gas-solid fluidized bed. AIChE Annual Meeting; 2013; San Francisco, CA, U.S.

160. Tsuji T, Miyauchi T, Oh S, Tanaka T. Simultaneous measurement of particle motion and temperature in two-dimensional fluidized bed with heat transfer. Kona Powder and Particle Journal. 2010(28):2-.

161. Brown SL, Lattimer BY. Transient gas-to-particle heat transfer measurements in a spouted bed. Experimental Thermal and Fluid Science. 2013;44:883-92.

162. Patil AV, Peters EAJF, Sutkar VS, Deen NG, Kuipers JAM. A study of heat transfer in fluidized beds using an integrated DIA/PIV/IR technique. Chem Eng J. 2015;259:90-106.

163. Tsuji T, Miyauchi, T., Oh, S., Tanaka, T. Simultaneous measurement of particle motion and temperature in two-dimensional fluidized bed with heat transfer. Kona Powder Part J. 2010;28:167-79.

164. Patil A, Peters E, Kuipers J. Comparison of CFD–DEM heat transfer simulations with

infrared/visual measurements. Chem Eng J. 2015;277:388-401.

165. Dang TYN, Kolkman T, Gallucci F, Annaland MV. Development of a novel infrared technique for instantaneous, whole-field, non invasive gas concentration measurements in gas-solid fluidized beds. Chem Eng J. 2013;219:545-57.

166. Dang TYN, Gallucci F, Annaland MV. Gas mixing study in freely bubbling and turbulent gas-solid fluidized beds with a novel infrared technique coupled with digital image analysis. Chem Eng Sci. 2014;116:38-48.

167. Zhong WQ, Zhang Y, Jin BS. Novel Method To Study the Particle Circulation in a Flat-Bottom Spout-Fluid Bed. Energ Fuel. 2010;24:5131-8.

168. Zhang Y, Zhong WQ, Jin BS. New method for the investigation of particle mixing dynamic in a spout-fluid bed. Powder Technol. 2011;208(3):702-12.

169. Moslemian D, Devanathan N, Dudukovic MP. Radioactive Particle Tracking Technique for Investigation of Phase Recirculation and Turbulence in Multiphase Systems. Rev Sci Instrum. 1992;63(10):4361-72.

170. Sanaei S, Mostoufi N, Radmanesh R, Sotudeh-Gharebagh R, Guy C, Chaouki J. Hydrodynamic Characteristics of Gas-Solid Fluidization at High Temperature. Can J Chem Eng. 2010;88(1):1-11.

171. Kondukov NB, Kornilaev, A. N., Skachko, I. M., Akhromenkov, A. A., Kruglov, A. S. . An investigation of the parameters of moving particles in a fluidized bed by a radioisotopic method. Int Chem Engng. 1964;4:43-7.

172. Lin JS, Chen MM, Chao BT. A Novel Radioactive Particle Tracking Facility for Measurement of Solids Motion in Gas-Fluidized Beds. Aiche J. 1985;31(3):465-73.

173. Kantzas A, Wright I, Bhargava A, Li F, Hamilton K. Measurement of hydrodynamic data of gas-phase polymerization reactors using non-intrusive methods. Catalysis Today. 2001;64(3-4):189-203.

174. Godfroy L, Larachi F, Chaouki J. Position and velocity of a large particle in a gas solid riser using the radioactive particle tracking technique. Can J Chem Eng. 1999;77(2):253-61.

175. Mostoufi N, Chaouki J. On the axial movement of solids in gas-solid fluidized beds. Chemical Engineering Research & Design. 2000;78(A6):911-20.

176. Mostoufi N, Chaouki J. Local solid mixing in gas-solid fluidized beds. Powder Technol. 2001;114(1-3):23-31.

177. Dudukovic MP. Opaque multiphase flows: experiments and modeling. Experimental Thermal and Fluid Science. 2002;26(6-7):747-61.

178. Hamidipour M, Mostoufi N, Sotudeh-Gharebagh R, Chaouki J. Experimental investigation of particle contact time at the wall of gas fluidized beds. Chem Eng Sci. 2005;60(15):4349-57.

179. Hamidipour M, Mostoufi N, Sotudeh-Gharebagh R, Chaouki J. Monitoring the particle-wall contact in a gas fluidized bed by RPT. Powder Technol. 2005;153(2):119-26.

180. Mabrouk R, Chaouki J, Guy C. Wall surface effects on particle-wall friction factor in upward gas-solid flows. Powder Technol. 2008;186(1):80-8.

181. Bhusarapu S, Al-Dahhan M, Dudukovic MP. Quantification of solids flow in a gas-solid riser: single radioactive particle tracking. Chem Eng Sci. 2004;59(22-23):5381-6.

182. Bhusarapu S, Cassanello M, Al-Dahhan MH, Dudukovic MP, Trujillo S, O'Hern TJ. Dynamical features of the solid motion in gas-solid risers. Int J Multiphas Flow. 2007;33(2):164-81.

183. Tamadondar MR, Azizpour H, ZarghamiA R, Mostoufi N, Chaouki J. Using particle trajectory for determining the fluidization regime in gas-solid fluidized beds. Adv Powder Technol. 2012;23(3):349-51.

184. Tamadondar MR, Zarghami R, Azizpour H, Mostoufi N, Chaouki J, Radmanesh R. Using S-statistic for investigating the effect of temperature on hydrodynamics of gas-solid fluidization. Particuology. 2013;11(3):288-93.

185. Schober L, Kantzas A. Analysis and interpretation of multiple radioactive particle tracking data on laboratory scale air/polyethylene fluidized beds. Can J Chem Eng. 2004;82(2):220-6.

186. Rasouli M, Bertrand F, Chaouki J. A Multiple Radioactive Particle Tracking Technique to Investigate Particulate Flows. Aiche J. 2015;61(2):384-94.

187. Bhusarapu S, Al-Dahhan MH, Dudukovic MP, Trujillo S, O'Hern TJ. Experimental study of the solids velocity field in gas-solid risers. Ind Eng Chem Res. 2005;44(25):9739-49.

188. Li YN, Fan H, Fan XF. Identify of flow patterns in bubbling fluidization. Chem Eng Sci. 2014;117:455-64.

189. Parker DJ, Dijkstra AE, Martin TW, Seville JPK. Positron emission particle tracking studies of spherical particle motion in rotating drums. Chem Eng Sci. 1997;52(13):2011-22.

190. Yang Z, Fan X, Fryer PJ, Parker DJ, Bakalis S. Improved multiple-particle tracking for studying flows in multiphase systems. Aiche J. 2007;53(8):1941-51.

191. Stein M, Ding YL, Seville JPK, Parker DJ. Solids motion in bubbling gas fluidised beds. Chem Eng Sci. 2000;55(22):5291-300.

192. Van de Velden M, Baeyens J, Smolders K. Solids mixing in the riser of a circulating fluidized bed. Chem Eng Sci. 2007;62(8):2139-53.

193. Van de Velden M, Baeyens J, Seville JPK, Fan X. The solids flow in the riser of a Circulating Fluidised Bed (CFB) viewed by Positron Emission Particle Tracking (PEPT). Powder Technol. 2008;183(2):290-6.

194. Chan CW, Seville J, Yang ZF, Baeyens J. Particle motion in the CFB riser with special emphasis on PEPT-imaging of the bottom section. Powder Technol. 2009;196(3):318-25.

195. Chan C, Seville J, Yang Z, Baeyens J. Particle motion in the CFB riser with special emphasis on PEPT-imaging of the bottom section. Powder Technol. 2009;196(3):318-25.

196. Hensler T, Tupy M, Strer T, Pöschel T, Wirth K-E. Positron emission particle tracking in fluidized beds with secondary gas injection. Powder Technol. 2015;279:113-22.

197. Mahmoudi S, Chan CW, Brems A, Seville J, Baeyens J. Solids flow diagram of a CFB riser using Geldart B-type powders. Particuology. 2012;10(1):51-61.

198. Parker DJ, Broadbent CJ, Fowles P, Hawkesworth MR, Mcneil P. Positron Emission Particle Tracking - a Technique for Studying Flow within Engineering Equipment. Nucl Instrum Meth A. 1993;326(3):592-607.

199. Fan XF, Parker DJ, Yang ZF, Seville JPK, Baeyens J. The effect of bed materials on the solid/bubble motion in a fluidised bed. Chem Eng Sci. 2008;63(4):943-50.

200. Chan CW, Seville J, Fan XF, Baeyens J. Solid particle motion in a standpipe as observed by Positron Emission Particle Tracking. Powder Technol. 2009;194(1-2):58-66.

201. Chan CW, Seville JPK, Parker DJ, Baeyens J. Particle velocities and their residence time distribution in the riser of a CFB. Powder Technol. 2010;203(2):187-97.

202. Laverman JA, Fan X, Ingram A, Annaland MV, Parker DJ, Seville JPK, et al. Experimental study on the influence of bed material on the scaling of solids circulation patterns in 3D bubbling

gas-solid fluidized beds of glass and polyethylene using positron emission particle tracking. Powder Technol. 2012;224:297-305.

203. Fan XF, Yang ZF, Parker DJ, Armstrong B. Prediction of bubble behaviour in fluidised beds based on solid motion and flow structure. Chem Eng J. 2008;140(1-3):358-69.

204. Hoomans BPB, Kuipers JAM, Salleh MAM, Stein M, Seville JPK. Experimental validation of granular dynamics simulations of gas-fluidised beds with homogenous in-flow conditions using Positron Emission Particle Tracking. Powder Technol. 2001;116(2-3):166-77.

205. van Buijtenen MS, Buist K, Deen NG, Kuipers JAM, Leadbeater T, Parker DJ. Numerical and experimental study on spout elevation in spout-fluidized beds. Aiche J. 2012;58(8):2524-35.

206. Mathiesen V, Solberg T. Laser-based flow measurements of dilute vertical pneumatic transport. Chem Eng Commun. 2004;191(3):414-33.

207. Mathiesen V, Solberg T, Hjertager BH. An experimental and computational study of multiphase flow behavior in a circulating fluidized bed. Int J Multiphas Flow. 2000;26(3):387-419.

208. McDonnel VG, Samuelsen, G. S. Evolution of the two-phase flow in the near field of an air-blast atomizer under reacting and non-reacting conditions. In: Adrian RJ, Asanuma, T., Durao, D., Durst, F., Whitelaw, J. H., editor. Applications of laser anemometry to fluid mechanics. New York: Springer-Verlag; 1989.

209. Zhang YF, Arastoopour H. Dilute Fluidized Cracking Catalyst Particles - Gas-Flow Behavior in the Riser of a Circulating Fluidized-Bed. Powder Technol. 1995;84(3):221-9.

210. Werther J, Hage B, Rudnick C. A comparison of laser Doppler and single-fibre reflection probes for the measurement of the velocity of solids in a gas-solid circulating fluidized bed. Chemical Engineering and Processing. 1996;35(5):381-91.

211. Mathiesen V, Solberg T, Arastoopour H, Hjertager BH. Experimental and computational study of multiphase gas/particle flow in a CFB riser. Aiche J. 1999;45(12):2503-18.

212. Ibsen CH, Solberg T, Hjertager BH. Evaluation of a three-dimensional numerical model of a scaled circulating fluidized bed. Ind Eng Chem Res. 2001;40(23):5081-6.

213. De Wilde J, Van Engelandt G, Heynderickx GJ, Marin GB. Gas-solids mixing in the inlet zone of a dilute circulating fluidized bed. Powder Technol. 2005;151(1-3):96-116.

214. Van Engelandt G, Heynderickx GJ, De Wilde J, Marin GB. Experimental and computational study of T- and L-outlet effects in dilute riser flow. Chem Eng Sci. 2011;66(21):5024-44.

215. Van Engelandt G, De Wilde J, Heynderickx GJ, Marin GB. Experimental study of inlet phenomena of 35 degrees inclined non-aerated and aerated Y-inlets in a dilute cold-flow riser. Chem Eng Sci. 2007;62(1-2):339-55.

216. Pantzali MN, Bayon NL, Heynderickx GJ, Marin GB. Three-component solids velocity measurements in the middle section of a riser. Chem Eng Sci. 2013;101:412-23.

217. Sasic S, Leckner B, Johnsson F. Characterization of fluid dynamics of fluidized beds by analysis of pressure fluctuations. Prog Energ Combust. 2007;33(5):453-96.

218. van Ommen JR, Mudde RF. Measuring the Gas-Solids Distribution in Fluidized Beds-A Review. Int J Chem React Eng. 2008;6.

219. van Ommen JR, Sasic S, van der Schaaf J, Gheorghiu S, Johnsson F, Coppens MO. Time-series analysis of pressure fluctuations in gas-solid fluidized beds - A review. Int J Multiphas Flow. 2011;37(5):403-28.

220. Rüdisüli M, Schildhauer T, Biollaz S, van Ommen J. Measurement, monitoring and control of fluidized bed combustion and gasification. In: Scala F, editor. Fluidized Bed Technologies for Near-Zero Emission Combustion and Gasification: Woodhead Publishing; 2013.

221. Davies CE, Fenton, K. Pressure fluctuations in a fluidized bed: a potential route to the continuous estimation of particle size. IPENZ Trans. 1997;24(1):12-20.

222. Chirone R, Miccio F, Scala F. Mechanism and prediction of bed agglomeration during fluidized bed combustion of a biomass fuel: Effect of the reactor scale. Chem Eng J. 2006;123(3):71-80.

223. Pitzer DR, Shabaker, R. H., Taylor, J. H., Tiller, M. L., Weinstein, H. Process for detecting, and monitoring changes in properties of fluidized bed solids by measurement of pressure difference fluctuation. Google Patents; 2000.

224. de Martín L, van Ommen J. Estimation of the overall mass flux in inclined standpipes by means of pressure fluctuation measurements. Chem Eng J. 2012;204-206:125-30.

225. Zhao GB, Yang YR. Multiscale resolution of fluidized-bed pressure fluctuations. Aiche J. 2003;49(4):869-82.

226. Briongos JV, Aragon JM, Palancar MC. Phase space structure and multi-resolution analysis of gas-solid fluidized bed hydrodynamics: Part I - The EMD approach. Chem Eng Sci. 2006;61(21):6963-80.

227. Briongos JV, Aragon JA, Palancar MC. Phase space structure and multi-resolution analysis of gas-solid fluidized bed hydrodynamics: Part II: Dynamic analysis. Chem Eng Sci. 2007;62(11):2865-79.

228. van Ommen J, van der Schaaf J, Schouten J, van Wachem B, Coppens M, van den Bleek C. Optimal placement of probes for dynamic pressure measurements in large-scale fluidized beds. Powder Technol. 2004;139:264-76.

229. Higashida K, Rai K, Yoshimori W, Ikegai T, Tsuji T, Harada S, et al. Dynamic vertical forces working on a large object floating in gas-fluidized bed: Discrete particle simulation and Lagrangian measurement. Chem Eng Sci. 2016;151:105-15.

230. Thess A, Votyakov E, Kolesnikov Y. Lorentz force velocimetry. Phys Rev Lett. 2006;96(16):1-5.

231. Viré A, Knaepen B, Thess A. Lorentz force velocimetry based on time-of-flight measurements. Phys Fluids. 2010;22:125101.

232. Wegfrass A, Diethold C, Werner M, Resagk C, Fröhlich T, Halbedel B, et al. Flow rate measurement of weakly conducting fluids using Lorentz force velocimetry. Meas Sci Technol. 2012;23(10):105307.

233. Halbedel B, Resagk C, Wegfrass A, Diethold C, Werner M, Hilbrunner F, et al. A novel contactless flow rate measurement device for weakly conducting fluids based on Lorentz force velocimetry. Flow Turbul Combust. 2014;92(1):361-9.

234. Medrano J, de Nooijer N, Gallucci F, van Sint Annaland M. Advancement of an Infra-Red technique for whole-field concentration measurements in fluidized beds. Sensors. 2016;16(3):300.

235. Yan Y. Flow rate measurement of bulk solids in pneumatic pipelines–problems and solutions. Bulk Solids Handling. 1995;15:447-56.

236. Sun JY, Zhou YF, Ren CJ, Wang JD, Yang YR. CFD simulation and experiments of dynamic parameters in gas-solid fluidized bed. Chem Eng Sci. 2011;66(21):4972-82.

237. Sun JY, Wang JD, Yang YR. CFD simulation and wavelet transform analysis of vortex and coherent structure in a gas-solid fluidized bed. Chem Eng Sci. 2012;71:507-19.